Aberrant immune regulation and enrichment of stem-like CD8$^+$ T cells in the pancreatic lymph node during type 1 diabetes development

Running title: Stem-like CD8$^+$ T cell phenotypes enriched in T1D

Leeana D. Peters[1, 2], Howard R. Seay[1, 2], Justin Smith[1, 2], Amanda L. Posgai[1, 2], Reed Berkowitz[1, 2], Clive H. Wasserfall[1, 2], Mark A. Atkinson[1, 2, 3], Rhonda Bacher[2, 4], Maigan A. Brusko[1, 2] and Todd M. Brusko[1, 2, 3, 5]*

[1]Department of Pathology, Immunology, and Laboratory Medicine, College of Medicine, University of Florida, Gainesville, FL, USA

[2]Diabetes Institute, University of Florida, Gainesville, FL, USA

[3]Department of Pediatrics, College of Medicine, University of Florida, Gainesville, FL, USA

[4]Department of Biostatistics, College of Public Health and Health Professions, University of Florida, Gainesville, FL, USA

[5]Department of Biochemistry and Molecular Biology, College of Medicine, University of Florida, Gainesville, FL, USA

*Correspondence to: Todd M. Brusko, Ph.D., Department of, College of Medicine, University of Florida, 1275 Center Drive, Biomedical Sciences Building J589, Box 100275, Gainesville, FL 32610. E-mail address: tbrusko@ufl.edu. TEL: (352) 273-9255. FAX: (352) 273-9339.

Conflict of Interest Statement: The authors declare no relevant conflicts of interest related to the work presented in this manuscript.

Word Count: 9159, Tables: 1, Figures: 7, Supplementary Tables:12, Supplementary Figures: 13

Summary

Effector CD8$^+$ T cells are key cellular drivers of type 1 diabetes (T1D) pathogenesis, yet questions remain regarding the molecular defects leading to altered cytotoxicity, their signature in peripheral tissues, and their receptor specificity. Thus, we analyzed human pancreatic lymph nodes (pLN) using mass cytometry and single cell RNA sequencing (scRNAseq) with combined proteomic and T cell receptor (TCR) profiling. Cytometric analysis revealed an enriched population of T stem-cell memory (TSCM)-like cells (CD8$^+$CD45RA$^+$CD27$^+$CD28$^+$CCR7$^+$CXCR3$^+$ T cells) in T1D pLNs. scRNAseq profiling indicated an elevated inflammatory cytokine gene signature (*IFITM3*, *LTB*) along with regulators of terminal differentiation (*BCL6*, *BCL3*), coupled with reduced expression of exhaustion-associated genes (*DUSP2*, *NR4A2*, *TSC22D3*) in CD8$^+$ T cells in T1D pLN. Additionally, effector CD8$^+$ T cells expressed features of progenitor exhausted cells (*BCL2*) in T1D pLN. Immune Response Enrichment Analysis (IREA) indicated IL-15 signaling as a significant driver of these phenotypes. Integrated TCR and transcriptomic analysis revealed a cluster of diverse naïve-like CD8$^+$ T cell clones in T1D pLN. When comparing pLN and pancreatic slice cellular isolates, we observed sharing of effector CD8$^+$ T cells, with upregulation of terminal effector signatures detected within the pancreas relative to paired pLN samples. Multiplex imaging revealed differential localization of TCF1 and TOX expressing T cells in the pancreas, with TCF1$^+$TOX$^+$ cells located in closer proximity to the islets and displaying a mixture of activation and exhaustion-associated phenotypes. Thus, we provide multimodal cellular profiles enriched in T1D tissues for consideration in therapeutic targeting.

Keywords: type 1 diabetes, human, pancreas, lymph node, CD8 T cell, single cell RNA sequencing

43 **Introduction**

44 Genetic fine mapping studies have identified that type 1 diabetes (T1D)-associated risk variants
45 preferentially localize to enhancer regions within immune cells, namely T and B cells[1]. However,
46 inaccessibility of the pancreas from living individuals mandates that studies examining immune cell
47 function in T1D largely be derived from peripheral blood, which may not accurately reflect phenotypes
48 within the target organ during disease pathogenesis. Identifying the molecular basis for T1D-associated
49 immune dysregulation within the pancreas and pancreatic draining lymph nodes (pLN) is highly valuable
50 in the process of developing targeted therapies.

51 The role of the pLN in promoting T1D progression is incompletely characterized, but murine and
52 human studies have implicated the pLN as an important priming site for immune activation[2-4]. In the non-
53 obese diabetic (NOD) mouse model of T1D, pLN self-renewing autoreactive T cells were found to be an
54 important source of islet antigen-specific cytotoxic lymphocytes[5]. Human studies indicate that patients
55 with T1D possess skewed T cell subset distributions within the pLN, with reduced T follicular regulatory
56 (TFR) cell frequency reported in one study[6] and increased Th17 cells noted in another[7]. Although there
57 are conflicting reports as to whether deficits in circulating regulatory T cell (Treg) number and function
58 are present in T1D patients[8, 9], multiple studies have demonstrated deficits in suppressive capacity[7] and
59 migration toward the pancreas[10] in Tregs derived from T1D pLN.

60 Though peripheral blood signatures do not always correlate with those from tissues[11], there have
61 been many important knowledge gains linking peripheral immunological signatures to clinical outcomes.
62 Interestingly, many of the signatures associated with immunotherapeutic response have converged
63 around $CD8^+$ T cell subsets. For example, an exhausted-like $CD8^+$ population expressing negative
64 regulatory molecules, including TIGIT and PD-1, together with exhaustion markers KLRG1 and CD57, was
65 associated with C-peptide preservation post-treatment with alefacept (LFA3-Ig)[12]. Similarly, expansion of
66 $TIGIT^+KLRG1^+CD8^+$ T cells was found preferentially in those who responded to teplizumab (α-CD3)[13].

67 Moreover, studies in mice[5] and humans[14, 15] have implicated $CD4^+$ and $CD8^+$ stem cell memory T cells
68 (TSCM) as a potentially important reservoir for promoting pathogenic antigen-specific responses in T1D.
69 Although clinical studies have shown that exhausted-like populations are clonally related to a different
70 $CD8^+$ memory population expressing more activation markers relative to exhaustion markers[12], there is a
71 paucity of information in T1D regarding the distribution of these subsets in secondary lymphatic organs
72 and pancreas, their receptor profiles, or the pathways driving these phenotypes.

73 Our lab has previously generated sorted T cell receptor (TCR) profiles from donor-matched pLN,
74 spleen, and peripheral blood samples, revealing cell type-dependent repertoire sharing across tissues,
75 with $CD8^+$ T cells demonstrating the greatest degree of sharing[16]. The advent of single cell profiling
76 technologies enables the examination of sharing between lymph node and pancreas T cell populations
77 with greater resolution. To understand the phenotypic and transcriptomic profile of immune cell
78 populations in disease-relevant tissues, we performed single cell multi-omic analysis of the pLN as well as
79 pancreatic T cells from donors with and without T1D. In this study, we show that circulating phenotypic
80 signatures previously identified to correlate with T1D status or immunotherapeutic response are shared
81 across tissue immune phenotypes. Moreover, we offer evidence that human $CD8^+$ T cells possess fewer
82 differentiated phenotypes in the pLN in T1D and that effector populations differentiate further upon
83 trafficking to the pancreas.

84 **Methods**

85 **Sex as a biological variable**

86 Male and female organ donors were accepted in this study.

87 **Human Organ Donors**

88 Tissues were recovered from T1D donors, donors possessing islet autoantibody positive (AAB+), as well as
89 donors without diabetes and negative for islet autoantibodies (ND) according to the Network for
90 Pancreatic Organ donors with Diabetes (nPOD) inclusion criteria[17]. Demographic information used to
91 stratify subjects for analyses was obtained from the nPOD datashare (https://npoddatashare.coh.org/)
92 and nPOD data portal (https://portal.jdrfnpod.org) websites. See **Table S1** for a description of cases and
93 corresponding experiment information.

94 **Organ Processing**

95 Tissues were processed as previously described[16]. Briefly, pLN were dissociated in HBSS + 10% human
96 (male, type AB) serum (Atlanta Biologicals) using a gentleMACS tissue processor (Miltenyi), followed by
97 subsequent homogenization and filtering steps using a tissue douncer (40 mL; loose pestle; Wheaton) and
98 100-µm, 70-µm, and 30-µm filters (Miltenyi) to obtain a single cell suspension. Cells were freshly analyzed
99 by flow cytometry as described below, and remaining cells were cryopreserved using CryoStor CS10
100 (Stemcell). Live pancreatic slices were prepared from nPOD organ donors as previously described[18] and
101 freshly digested with 1X collagenase IV (Stemcell) diluted in DMEM for 30 minutes at 37°C and 5% CO_2.
102 Remaining tissue was gently mechanically dissociated with frosted slides and filtered using 70-µm filters
103 (Miltenyi) to obtain a single cell suspension. Cells were enriched for $CD45^+$ cells using CD45 Microbeads
104 (Milltenyi) and processed for scRNAseq (10X Genomics) as below.

105 **Flow Cytometry**

106 Fresh tissues were dissociated as above and stained with Live/Dead yellow viability dye (Invitrogen) and
107 incubated with TruStain FcX (Biolegend) according to the manufacturer's instructions prior to staining
108 with a panel of antibodies broadly examining memory, effector, and naïve immune cell phenotypes (**Table**
109 **S2**) consistent with previously published methods[19]. Data were acquired on an LSRFortessa (BD). To assess
110 expression of transcription factors TCF1 and TOX in $CD8^+$ T cell populations, cryopreserved pLN cell
111 suspensions were thawed, stained with Zombie Aqua viability dye (Invitrogen), incubated with TruStain
112 FcX (Biolegend), and stained with antibodies (**Table S3**). After extracellular staining, cells were washed
113 with stain buffer (PBS, 2% FBS, 0.05% NaN3) twice prior to fixation and permeabilization using the True
114 Nuclear Transcription Factor Buffer Set (Biolegend) according to manufacturer instructions. Cells were
115 blocked with normal rat serum prior to staining for transcription factors overnight at 4°C in
116 permeabilization buffer. Cells were washed with stain buffer prior to reading on a Cytek Aurora 5L
117 cytometer. For analysis of cytokine expression, cryopreserved pLN suspensions were thawed and
118 incubated at a concentration of 1e6/mL with Cell Stimulation Cocktail (Invitrogen) in the presence of
119 0.66μL/mL GolgiStop (BD) for four hours. Cells were stained with Zombie Aqua (Invitrogen), incubated
120 with TruStain FcX (Biolegend), and stained with a panel of antibodies (**Table S4**). After extracellular
121 staining, cells were fixed with BD cytofix and permeabilized with Intracellular Staining Perm Wash Buffer
122 (Biolegend). Staining for cytokines was conducted overnight at 4°C in perm wash buffer. Cells were
123 washed with perm wash buffer prior to reading on a Cytek Aurora 5L cytometer. Data were analyzed
124 using FlowJo V10.8.2 software.

125 **Mass Cytometry**

126 Cryopreserved cells from pLN of ND (n=12) and T1D donors (n=10) were stained with a 35-marker panel
127 (**Table S5**) of MAXPAR metal-chelating polymers and run on a CyTOF mass cytometer by the Human

128 Immune Monitoring Center at Stanford University, as reported previously[20].

129 **Mass Cytometry Analysis Pipeline**

130 Data were normalized between batches using premessa[21] in R based on internal bead controls. After this,
131 FCS files were loaded into FlowJo (BD Biosciences), beads were excluded, and live single $CD45^+$ cells were
132 used for downstream analysis (**Figure S1**). Data analysis involved importing FCS files into R and creating a
133 flowset using the flowCore package[22]. Data were arcsinh transformed with a cofactor of 5 prior to using
134 the expression data and cell metadata to create a Seurat object. Principal component analysis (PCA) was
135 run using all panel markers, after which K nearest neighbors (KNN) were calculated using FindNeighbors(),
136 and initial clustering using the lovain algorithm was performed (resolution=0.2). PCA was re-run on
137 subsetted data with markers not associated with the lineage of interest removed. Nearest neighbors were
138 calculated as above, and subclustering was performed as above for each subset using the Louvain
139 algorithm (resolution=0.2). Cell counts per cluster per individual were determined and normalized by the
140 total number of cells to allow for comparison of cluster proportions. Differential abundance analysis was
141 performed using propeller[23] with age and batch as covariates in a linear model designed with
142 model.matrix(~0 + group + age + Batch). Design matrix and contrasts (T1D-ND) were incorporated into
143 the propeller.ttest function with arguments robust=T, trend=F, sort=T. Significantly altered cluster
144 proportions were defined as Bonferroni adjusted p-value <0.05.

145 **Single Cell RNA Sequencing**

146 Cryopreserved single cell suspensions were thawed and stained with a cocktail of 7 oligo-barcoded
147 TotalSeq antibodies (Biolegend, **Table S6**) and peptide-MHC dextramers (Immudex, **Table S6**) to aid in
148 clustering naïve and memory $CD8^+$ and $CD4^+$ T cell phenotypes and to aid in identification of antigen-
149 specific cells. Prior to use, Totalseq antibodies were centrifuged at 14000x*g* for 10 minutes at 4°C to avoid

150 antibody aggregates, as recommended by the manufacturer. Cell viability was assessed using acridine
151 orange and propidium iodide (AO/PI) staining on a Nexcelom Cellometer or CellDrop. For six samples with
152 viability <70% (**Table S7**), the Dead Cell Removal Kit (Stemcell) was used. $1x10^6$ cells per sample (viability
153 >70%) were resuspended in 100μL volume of PBS + 1% BSA prior to incubation with 2μL of each pMHC
154 dextramer according to manufacturer's instructions for 10 minutes at room temperature (RT), followed
155 by incubation with TruStain FcX (5μL/test) to block Fc receptors for 10 minutes at 4°C, and incubation with
156 the antibody master mix (0.5μL of each antibody/test) for 30 minutes at 4°C. Cells were washed four times
157 with 3mL of chilled PBS + 1% BSA, after which live cells were counted using AO/PI on a Nexcelom
158 Cellometer or CellDrop, and volumes adjusted to obtain a targeted recovery of 10,000 cells. Single cell
159 suspensions were loaded into the Chromium Controller (10X Genomics) and libraries prepared according
160 to the 5' v1.1, 5' v2, and 5' HT v2 kit protocols (10x Genomics). Libraries were sequenced on an Illumina
161 Novaseq or Novaseq X instrument with a target of 50,000 paired reads for gene expression, 10,000 paired
162 reads for surface protein, and 5,000 paired reads for TCR libraries. Median gene expression library
163 sequencing saturation was 80.9%.

164 **Single Cell Read Processing**

165 BCL files were processed to fastq files using the cellranger mkfastq pipeline (10X Genomics). Fastq files
166 from gene expression, surface protein, and TCR libraries were processed to matrices using the cellranger
167 multi (10X Genomics) count pipeline in order to maximize counting of cells with all three modalities.

168 **Single Cell RNAseq Normalization and Analysis Pipeline**

169 scRNAseq data were subject to quality control (QC) by removing doublets using the doubletfinder
170 package[24], and cells were removed based on cutoffs of reads/cell ≤2000 and percent mitochondrial reads
171 ≤10%, then normalized using the DSB package[25] to remove background noise and ambient signal from

172 RNA and protein libraries. After this initial filtering, data were log-normalized with NormalizeData() and
173 scaled with ScaleData(), then variable features were calculated, and dimensionality reduction was
174 performed in Seurat[26]. Due to a lack of observed pMHC dextramer signal, we excluded these from future
175 analysis. For the antibody-derived tag data, variable features were set to all antibodies included, data
176 were scaled[26], and PCA was run. Data were integrated in Seurat using IntegrateLayers() with RPCA as the
177 integration method. After integration of gene expression data by patient ID, we observed no significant
178 batch effects (**Figure S2**). After subsetting T cell clusters, data were renormalized, PCA was rerun, and
179 RPCA integration with IntegrateLayers() was run again on this subset. Integration of TCR with gene
180 expression data was performed using scRepertoire[27] in R. For pancreas and pLN clone comparison, clones
181 were defined as sequences sharing an identical complementarity determining region 3 (CDR3) amino acid
182 sequence for both TCRα and TCRβ. Differentially expressed genes (DEGs) were calculated using MAST[28]
183 with sex as a latent variable with a minimum expression threshold of 0.10 and reported when false
184 discovery rate (FDR) corrected $p<0.05$ and log2 fold change (FC)$\geq$0.26. Pathway enrichment analyses were
185 performed using the top 100 most differentially expressed genes (other than for the exhausted CD8 T cell
186 cluster for which only 53 genes met our significance thresholds) between T1D and ND donors, with FDR
187 $p<0.05$ per cluster ranked by log2FC, as input into the ReactomePA[29] package for pLN. The R package
188 escape[30] was used to perform single-sample Gene Set Enrichment Analysis (ssGSEA) using the integrated
189 pancreas and pLN dataset and normalized with nFeature RNA as the scale factor. Results were reported
190 when Benjamini-Hochberg corrected $p<0.1$ as noted in figure legends. IREA analysis was performed by
191 inputting the top ($p<0.05$, log2FC >0.26) DEGs between T1D and ND donors per cluster using the IREA web
192 tool (https://www.immune-dictionary.org/app/home) with cell type of "T_cell_CD8", species of "Human"
193 and Method parameter of "Score".

194 **Clonotype Neighbor Graph Analysis (CoNGA)**

195 The RNA assay from the integrated pLN Seurat object was exported in h5ad format for Python. Filtered
196 contig annotation data from each sample were merged using make_10x_clones_file_batch from the
197 conga package in Python. The resulting merged TCR data were used along with the gene expression data
198 as input for run_conga.py[31] with the –all flag and batch keys set to status and nPOD identification number
199 (ID) in order to compare the composition of clusters by clinical status and across all donors. Gene
200 expression data were also batch corrected using the argument batch_integration_method harmony with
201 batch_integration_key batch. For CONGA analyses, the cellranger VDJ clonotype definition of identical
202 CDR3 nucleotide sequence was used. Clones that possessed a conga score<1, indicative of significant
203 overlap between gene expression and TCR neighborhoods beyond what would be expected by chance[31],
204 were used as input to evaluate enrichment in cluster composition by clinical status using two-sided
205 Fisher's exact test as reported in the figure legend.

206 **Phenocycler multiplex imaging**

207 Immunofluorescence of pancreas with embedded lymph node was performed using the PhenoCycler-
208 Fusion System (Akoya Biosciences/Quanterix) according to the vendor's recommended protocol for
209 formalin fixed paraffin embedded (FFPE) tissue. Deparaffinization was performed by baking at 60°C
210 followed by xylene washes. Tissue rehydration was accomplished by moving the slide through graded
211 ethanol/DI-H_2O washes (100%x2, 90%, 70%, 50%, 30%, DI-H_2Ox2). Antigen retrieval was performed by
212 immersing sections in 1X antigen retrieval buffer under high pressure in a pressure cooker. Tissue was
213 then washed in Hydration Buffer and then Staining Buffer. Primary antibody staining was performed using
214 175µL of antibodies (**Table S7**), blocking reagents (N, G-v3, J, S), and blocking buffer cocktail at RT. The
215 tissue was then rinsed in Staining Buffer and sequentially post-fixed, followed by PBS washes, in 1.6%
216 paraformaldehyde, then ice-cold methanol, and finally Fixative Solution. Tissue was then kept overnight
217 in Storage Buffer at 4°C. The following day, a 96-well reporter plate was prepared with either cycle-specific

218 cocktails of complementary oligonucleotide-conjugated fluorescent secondaries, Nuclear Stain (DAPI),
219 and Reporter Stock Solution for cyclic protein detection or only Reporter Stock Solution for blank cycle
220 autofluorescence detection. Finally, a Flow Cell was press-sealed to the face of the slide for microfluidic
221 delivery of reagents.

222 Automated detection and imaging were performed by first generating an experiment file specifying
223 target-barcode pairs and exposure times for each cycle (Experiment Designer software, Akoya
224 Biosciences/Quanterix). Phenocycler Buffer and dimethyl sulfoxide solutions (20% and 90% in 1X
225 Phenocycler Buffer) were prepared and loaded in the Phenocycler-Fusion instrument bottles. Following
226 automated calibration and equipment checks, tissue was auto-detected, and images were acquired with
227 16-bit precision at 20x magnification, automatically processed for stitching and autofluorescence
228 subtraction, and saved in the proprietary 'qptiff' format.

229 **Phenocycler data analysis**

230 Semantic segmentation was performed in QuPath[32]v6.0 T on the qptiff file for donor 6551. Objects
231 (pLN/Pancreas tissue area and islets) were classified using the pixel classifier with default settings. Cell
232 and nuclear boundaries were generated with the Instanseg[33]v0.1.5 extension's default model
233 "fluorescence_nuclei_and_cells-0.1.1" using all channels as input, default cell measurements, and default
234 outputs. Statistics for each cell's shape and marker intensity, as well as centroid coordinates and signed
235 distance to nearest islet, were exported as a csv file for analysis in a custom Python Jupyter notebook[34].

236 **Statistics**

237 Data were analyzed using R v4.2.3, python v3.9 and GraphPad Prism v9. Statistical tests and p-values are
238 reported in the figure legends.

239 **Study approval**

240 The study was conducted in accordance with federal guidelines and the University of Florida (UF)
241 Institutional Review Board approved protocol IRB201600029, as previously described[35].

242 **Data and code availability**

243 Mass cytometry and flow cytometry data are available at ImmPort (https://www.immport.org, accession
244 number: SDY3066). Supporting Data Values associated with this manuscript are provided in the
245 supplement. Gene expression and TCR data are available on GEO with accession: GSE298811. Phenocycler
246 data are available upon request, and code used for Phenocycler analysis can be accessed at
247 https://github.com/smith6jt-cop/Panc_pLN_Analysis.

248

249 **Results**

250 **Mass cytometry reveals a population of CD8$^+$CXCR3$^+$ T cells enriched in T1D pLN**

251 The diverse nature of immune cell phenotypes mandates the use of high-parameter technologies, such as
252 cytometry time of flight (CyTOF)[36, 37 12], to deep-phenotype multiple immune subsets. We applied high-
253 parameter CyTOF to pLN derived from 10 T1D and 12 ND nPOD organ donors (**Table S8, Figure 1A**).
254 Clustering total CD45$^+$ immune cells revealed 11 unique populations spanning B cells, CD4$^+$ T cells, CD8$^+$ T
255 cells, myeloid, and natural killer (NK) cells (**Figure S3A**). We observed no significant differences in cluster
256 abundance globally between T1D and ND donors (**Figure S3B**);

257 We performed subclustering to obtain a finer resolution of immune cell subsets from the CyTOF
258 data. As one batch demonstrated slight, non-significant differences in age (**Figure S4**), we chose to
259 examine differences in cluster proportions using a linear model with age and batch incorporated as

260 covariates. Subsetting and reclustering of B cells and CD4 T cells yielded no significant changes in cluster
261 abundance or marker expression by clinical status (**Figure S5**). However, $CD8^+$ T cell subclustering yielded
262 eight proteomic clusters (**Figure 1B**), with a T1D-associated increase in the proportion of $CD8^+$ T cell cluster
263 0, expressing the naïve T cell markers CD45RA and CCR7, costimulatory molecules CD27 and CD28, as well
264 as low levels of the chemokine receptor CXCR3, which confers migratory capacity towards CXCL10[38]
265 (**Figure 1C-D**). Though we observed more variability due to the small number of donors, this finding was
266 also confirmed in an independent flow cytometry cohort consisting of 23 nPOD pLN cell isolates from ND,
267 autoantibody positive (AAB+) and T1D donors (**Table S9**) (**Figure 1E, Figure S6**), where T1D donors
268 possessed a significantly increased proportion of $CXCR3^+$ cells within the naïve ($CD45RA^+CCR7^+$) $CD8^+$ T cell
269 compartment as compared to both ND (p=0.0114, FC=2.50) and AAB+ donors (p=0.0090, FC=4.91).
270 Importantly, we did not observe an association of the frequency of this cluster or the related flow
271 cytometry phenotype with age or disease duration (**Figure S7A-D**). These phenotypic signatures are
272 clinically relevant in peripheral blood studies: we recently reported a T1D-associated increase in $CXCR3^{lo}$
273 naïve $CD8^+$ T cells[19], and circulating $CD8^+$ T cells with a more terminally differentiated/exhausted profile
274 have been previously correlated with preservation of C-peptide and response to teplizumab[12, 13].

275 **IL-15 drives memory maintenance and averts the exhaustion program in T1D $CD8^+$ T cells**

276 To explore the transcriptomic profile of the cell populations previously identified by both CyTOF and
277 fluorochrome-based flow cytometry, we performed single cell RNA sequencing (scRNAseq) analysis with
278 TCR-seq on donor pLN (**Figure 2A**). After QC, we obtained 122,300 cells across 16 individuals (9 T1D, 7 ND)
279 (**Table S10**) that comprised 38 clusters spanning $CD4^+$ T cells, $CD8^+$ T cells, B cells, NK cells, innate lymphoid
280 cells (ILCs), monocyte/macrophages, and dendritic cells (DCs) (**Figure 2B**, **Figure S8A-B**). No significant
281 differences in global cluster abundance across clinical status were detected (**Figure S8C-D**). We performed
282 subclustering to more deeply examine alterations in T cell phenotype, yielding 19 subclusters spanning

283 naïve, memory, and exhausted T cells, as well as Tregs (**Figure 2C**). Differential expression analysis of T1D
284 compared to controls identified conserved signatures across multiple CD4 T cell clusters, such as a
285 reduction in genes responsible for negative regulation of cytokine signaling (e.g., *TNFAIP3*[39] within naïve
286 CD4, T follicular helper [TFH], Th1/17, thymic Treg [tTreg] clusters) and activation/proliferation (e.g.,
287 *JUND*[40] within TFH, tTreg, Th1/17, Th17 clusters), as well as a broad increase in interferon signaling genes
288 (e.g., *IFITM3*[41] within Th17, naïve CD4, exhausted CD4, activated naïve CD4, TFH, Th1/17) (**Table S11**).

289 We next focused more deeply on $CD8^+$ T cell subsets as these phenotypes were significantly
290 altered in our CyTOF and flow cytometry data. When comparing DEGs (defined as FDR corrected $p<0.05$
291 and $Log2FC \geq 0.26$) between T1D and ND pLN, we observed within the naïve $CD8^+$ T cell cluster (**Figure 2D**)
292 an upregulation of genes involved in autophagy (*MAP1LC3B*[42], *SQSTM1*[43]), migration (*VIM*), proliferation
293 (*IMPDH2*[44]), and cytokine production (*TAGLN2*[45]). CD8 TCM cells from T1D donors showed upregulation
294 of inflammatory cytokine signaling (*IFNAR2*[46], *IFITM3*, *LTB*[47], *SOCS3*[48], *IL32*[49], *IL27RA*[50]) as well as regulators
295 of terminal differentiation (*BCL3*[51], *BCL6*[52], *BATF*[53]). Moreover, both naïve and TCM $CD8^+$ T cells from T1D
296 donors also downregulated genes involved in negative regulation of cytokine signaling (*TNFAIP3*[39],
297 *SOCS1*[54]) and genes associated with T cell exhaustion (*DUSP2*[55], *NR4A2*[56], *TSC22D3*[57]) as compared with
298 ND. In the CD8 effector T cell (Teff) cluster (**Figure 2D**), we observed an upregulation of genes involved in
299 effector function (*SLC3A2*[58], *NKG7*[59]), as well as migratory genes (*VIM*[60], *ITGA1*[61]) in T1D relative to ND
300 donors. We also noted upregulation of the anti-apoptotic factor *BCL2*, which is important for the
301 maintenance of long-lived memory subsets[62, 63], within CD8 Teff in T1D. Moreover, within this cluster, we
302 observed downregulation of genes associated with terminal differentiation and exhaustion (*CXCR4*[64],
303 *DUSP2*[55]), indicative of restraining of terminal differentiation in T1D as compared to controls. Similarly, in
304 the exhausted CD8 T cell cluster (CD8 Texh) (**Figure 2D**), we observed upregulation of genes involved in
305 migration (*VIM*[60]), calcium signaling (*S100A6*, *S100A11*[65]), inflammatory cytokine response (*SOCS3*,
306 *IFITM1*, *IFITM3*, *IFITM2*[41, 66]), and cytotoxicity (*HMGN2*[67], GZMM), while genes associated with terminal

307 differentiation and exhaustion (*TSC22D3, DUSP2*, *HLA-DQB1*[68]) were downregulated in T1D. We did not
308 detect differential expression of other canonical markers of stemness or exhaustion (i.e., *TCF7*, *LEF1*,
309 *CD122*, *CXCR3*, *PD1*), potentially due to data sparsity or differential regulation of protein and RNA
310 expression.

311 Pathway analysis using the Reactome database revealed that naïve CD8 T cells (**Figure S9A**) in T1D
312 were enriched for autophagy and mitophagy. Additionally, CD8 TCM cells in T1D were enriched for
313 interleukin signaling and interferon signaling (**Figure 2E**), while CD8 Teff (**Figure 2F**) were enriched for
314 interleukin signaling and smooth muscle contraction, the latter likely reflective of increased calcium
315 signaling (*ANXA1*, *ANXA2*)[69]. Lastly, CD8 Texh (**Figure 2G**) were enriched for interferon signaling,
316 interleukin signaling, and signal transduction through growth factor receptors (*TGFB1*, *FLT3LG*[70]) and
317 second messengers (*PIM1*[71]). We then performed Immune Response Enrichment Analysis (IREA), which
318 uses an extensive database of specific gene sets induced by cytokine treatment[72], to infer the cytokine
319 milieu driving these CD8 phenotypes. Across the trajectory of $CD8^+$ T cell differentiation, IL-15 signaling
320 was notably enriched in T1D (**Figure S9B**; **Figure 2H-J**), a pathway that is known to promote stemness and
321 restrain exhaustion-like phenotypes[73] and can synergize with other inflammatory cytokines to promote
322 effector function[74]. Collectively, these data and our prior peripheral blood findings[75] suggest Tc1 skewing
323 as an immunological feature of T1D shared across tissues.

324 **$CD8^+$ T cell clones possessing naïve-like and *$TCF7^+$*TOX^+ phenotypes are more prevalent in T1D pLN**

325 Separate analyses of receptor or transcriptomic data may preclude insights into the relationships between
326 repertoire characteristics and phenotype. Thus, recent methods have been developed to enable joint
327 analysis of these modalities, namely Clonotype Neighbor Graph Analysis (CoNGA)[31], which has shown
328 utility in revealing transcripts associated with specific TCR genes and features. We applied CoNGA to our
329 pLN dataset, which identified 35 groups with significant (CoNGA score <1) overlap in TCR and gene

330 expression neighborhoods and a minimum of 4 cells per group (**Figure S10**). In accordance with the
331 original CoNGA publication[31], we found a stronger relationship between receptor and phenotypes in $CD8^+$
332 T cells and invariant T cells, with the majorityof our CoNGA hit clusters being comprised of $CD8^+$ T cells,
333 including naïve, effector, and mucosal-associated invariant T (MAIT) cell clusters (**Figure S10**). Among
334 these clusters, we found 10 that were overrepresented to some degree in T1D donors (**Figure 3A**,
335 indicated by leftmost orange bar). In particular, we observed that CoNGA clone hits belonging to CoNGA
336 gene expression (GEX) cluster 8 and TCR cluster 4 were found in several T1D donors, the highest frequency
337 being found in new-onset donor 6550, while 37/38 clones detected in ND donors (97%) were found in a
338 single ND donor possessing high risk HLA alleles (HLA A*0201, HLA DRB1*0401) (**Table S12)**. Thus, clones
339 belonging to these clusters were more often found in T1D (p=0.0012, OR=1.988) (**Figure 3B**). The enriched
340 GEX cluster 8/TCR cluster 4 is comprised of $CD8^+$ T cells with high TCR diversity (113 unique clonotypes
341 and 113 total cells, indicative of no clonal expansion) and with high expression of *CCR7*, *SELL*, *LEF1*, *TCF7*,
342 and *IL7R*. We also noted that this cluster possessed some features suggesting prior activation, namely
343 *KLRK1*[76], costimulatory molecule *HCST*[77] encoding DAP10, and low *CXCR3* expression. The TCRs within this
344 cluster possessed a diverse TCR beta chain (*TRB*) repertoire, while alpha chain (*TRA*) gene usage was
345 restricted to TRAV14/DV4, TRAV38-2/DV8, and TRAV38-1 (**Figure 3A**). Additionally, this cluster also
346 possessed a low Atchley factor 4 score (blue af4 logo, TCRseq features panel, **Figure 3A**), which has
347 previously been associated with larger, more hydrophobic residues[31]. In addition to this naïve-like cluster,
348 we also noted enrichment of a less frequent cluster (GEX cluster 11, TCR cluster 13), which possessed a
349 more terminally differentiated profile, expressing cytotoxicity markers (*GZMA*, *GZMK*, *NKG7*),
350 costimulatory molecule *HCST*, as well as *CXCR3* and both *TCF7* and *TOX* (**Figure 3A**). Though infrequent,
351 this cluster was also present in multiple T1D donors, with only 2/18 clones being found in ND donors. We
352 searched for known T1D clones[78] in these T1D-associated CoNGA clusters based on similarity to known
353 alpha chain complementary determining region 3 (CDR3) sequence, given recent data on potential alpha

354 chain biases in autoreactive clones in T1D[79]. We found within the naïve-like cluster several clones which
355 share CDR3a (allowing for one amino acid mismatch) with known T1D clones, namely four GAD65 reactive
356 clones, three preproinsulin reactive clones, and a clone which possessed a CDR3a chain shared across
357 multiple specificities in a new onset T1D donor. We also found three clones with matching CDR3a to clones
358 with GAD65, $ZNT8_{186-194}$ and PPI_{16-25} specificities in a control donor with high-risk HLA alleles (**Table S12**).
359 In the more terminally differentiated cluster, we found an expanded clone (clone size of 6) matching a PPI
360 reactive clone, as well as sharing an alpha chain motif "AGGYQKVTF" present in the previously published
361 22.A10[80] PPI_{1-11} reactive clone (**Table S12**). Thus, these enriched clusters may contain autoreactive
362 specificities. Interestingly, we also noted an increase (p=0.0007, OR=2.153) in a group of expanded TCRs
363 (CoNGA gene expression cluster 16 paired with TCR cluster 13) comprised of MAIT and semi-invariant T
364 cells (*TRAV1-2* gene usage paired with a more diverse set of *TRB* chains) in T1D pLN (**Figure S11**).

365 **Shared memory T cell populations demonstrate enhanced effector phenotype in pancreatic slices**

366 To investigate receptor sharing and gene expression across tissues, we performed scRNAseq on isolated
367 immune cells from fresh pancreatic slices[81, 82] and paired pLN (**Figure 4A**) from 2 recent-onset T1D donors
368 (nPOD 6551, duration 0.58 years; nPOD 6536, duration 4 years) with independently confirmed insulitis[83].
369 Data integration yielded 17 clusters, which included naïve, memory, and effector $CD4^+$ and $CD8^+$ T cell
370 populations, Tregs, B cells, and resident macrophage populations (**Figure 4B**). We first interrogated the
371 TCR repertoire to examine sharing of T cell clones across these tissues, and while both donors possessed
372 insulitis, the newer onset donor 6551 possessed more extensive insulitis than donor 6536 (**Figure 4C**). We
373 found that expanded clones localized mostly to clusters 0 (CD8 Teff) and 2 (CD8 CTL), respectively
374 corresponding to $CD8^+$ T cell populations with lower and higher expression of cytotoxicity-related
375 molecules (*GZMK*, *CST7*, *LTB*) (**Figure 4D-E**). Clone sharing across pancreas and pLN was minimal, with
376 morisita horn (MH) values of 0.007 and 0.002 for cross-tissue overlap for donors 6536 and 6551,

377 respectively (**Figure 5F**). However, even with our limited sample size, we were able to detect 6 unique
378 clonotypes shared across tissues and clusters, with 2 clones shared across tissues (**Figure 4G, Table 1**). We
379 detected an expanded $CD4^+$ T cell clone in donor 6536, which was shared between tissues (cluster 9, $ICOS^{hi}$
380 TCM), as well as an expanded $CD8^+$ T cell clone in donor 6551, which was shared between tissues (clusters
381 0/2 CD8 Teff and CTL). The majority of sharing was detected between the effector CD8 clusters 0 and 2,
382 especially within donor 6551, as compared to donor 6536, perhaps due to reduced infiltration as a result
383 of increased disease duration.

384 We next investigated tissue-specific phenotypic differences in these clusters. We noted that $CD8^+$
385 Teff clusters 0 and 2, defined by expression of NK cell receptors (*KLRK1*[84], *KLRB1*[85]), Th1 related chemokine
386 receptors and ligands (*CXCR3*, *CXCR6*, *CCL5*[86]), and markers of terminally differentiated memory subsets
387 (*LAG3*, *KLRD1*, *EOMES*[87]), were the most commonly shared clusters across tissues, while less differentiated
388 subsets, such as naïve T cells, were expectedly more prevalent in pLN. Additionally, inflammatory
389 macrophages expressing *IL1B* were more prevalent in pancreas (**Figure 5A**). Examining DEGs of total CD8
390 T cells between tissues revealed increased expression of genes involved in promoting naïve/stem-like
391 phenotypes, *LEF1* (Log2FC=4.8, $p_{adj}=1.6e^{-7}$) and *SELL* (Log2FC=4.0, $p_{adj}=1.4e^{-}7$), in pLN relative to pancreas
392 (**Figure 5B**). As this could partially be explained by the increased proportion of naïve cells in pLN relative
393 to pancreatic slice, we sought to compare gene expression of shared populations across tissues. We found
394 that cells from cluster 0 (CD8 Teff) derived from pancreatic slices expressed enhanced markers of
395 cytotoxicity, such as *GZMB* (Log2FC=5.46, $p_{adj}=1.4e^{-46}$) as well as exhaustion marker *DUSP4*[88] (Log2FC=6.6,
396 $p_{adj}=1.3e^{-57}$) alongside reduced expression of common gamma chain cytokine receptors *IL7R (*Log2FC=-1.9,
397 $p_{adj}=2.5e^{-10}$) and *IL2RG* (Log2FC=-2.0, $p_{adj}=4.1e^{-5}$) (**Figure 5C**). Cluster 2, which possessed a similar
398 transcriptomic profile to cluster 0 but with enhanced expression of cytotoxicity and memory markers (CD8
399 CTL), demonstrated similar transcriptomic expression differences as cluster 0 across tissues (**Figure 5D**).
400 GSEA of cluster 0 revealed upregulation of inflammatory signaling pathways, namely IL-6-JAK-STAT3

401 (Log2FC=2.3, p_{adj}=1.5e^{-19}) and TNFα signaling (Log2FC=0.34, p_{adj}=1.7e^{-7}), as well as downregulation of Wnt-
402 Beta catenin signaling (Log2FC=-0.6, p_{adj}=2.3e^{-3}) (**Figure 5E**) in pancreatic slices compared to pLN,
403 altogether suggesting that this cluster acquired a more differentiated transcriptomic program in pancreas
404 relative to pLN. We observed similar upregulation of inflammatory pathways in cluster 2, representing an
405 activated effector phenotype (**Figure 5F**). Notably, while Wnt-Beta catenin signaling was not significantly
406 enhanced in pLN for this cluster, we did observe upregulation of *GIMAP5*[89] (Log2FC=-3.3, p_{adj}=1.5e^{-8}) in
407 pLN, which is an important negative regulator of GSK3β and thus, potentially enhances Wnt-signaling. In
408 line with prior observations of IL-15 signaling in the pancreas, IREA analysis of DEGs from CD8$^+$ T cell
409 clusters 0 and 2 between pLN and pancreas revealed enriched IL-15 signaling as a driver of differential
410 tissue phenotypes (**Figure S12**).

411 **CXCR3$^+$ naïve T cells show features of stemness and polyfunctionality in the pLN**

412 In order to more deeply understand the phenotype and function of the naïve CXCR3$^+$ cells (cluster 0) we
413 identified as being enriched in T1D pLN, we examined the expression of canonical exhaustion and TSCM
414 markers on pLN CD8 T$^+$ cells in a cohort of 5 T1D and 5 control donors by flow cytometry. We confirmed
415 that CXCR3$^+$ naïve CD8$^+$ T cells, along with the remainder of the naïve cells (CXCR3- naïve), express
416 significantly more TCF1 (p=0.0003, FC=2.04), and possess a significantly greater fraction of TCF1$^+$ cells than
417 memory cells (**Figure 6A-B**, **Figure S13**). We also observed that TSCM (CD45RA$^+$CD45RO$^-$CXCR3$^-$
418 CD95$^+$CD27$^+$) and CXCR3$^+$ naïve CD8$^+$ T cells express similar levels of TOX, with both populations displaying
419 increased expression of TOX relative to naïve cells (TSCM: p=0.0130, FC=1.21; naïve CXCR3$^+$: p=0.0013,
420 FC=1.19) (**Figure 6C**). Interestingly, we also noted increased TCF1 expression on naïve CXCR3$^+$ cells from
421 T1D donors relative to control donors (**Figure 6D**) (p=0.0317, FC=1.81). Supporting the notion that these
422 cells possess a transitional phenotype, TCF1$^+$ cells expressed significantly increased expression of CD127
423 as compared to TCF1$^-$ cells (p=0.0107, FC=1.32), as well as reduced PD-1 expression (p=0.0003, FC=0.80),

424 and enhanced CD5 expression ($p<0.0001$, FC=1.85) (**Figure 6E-G**). Moreover, after four hours of
425 stimulation with PMA/ionomycin, we found that naïve CXCR3$^+$ cells upregulated IL-2 and TNFα as
426 compared to the remainder of naïve (CXCR3-) cells (IL-2: $p=0.0002$, FC=3.11; TNFα: $p=0.0006$, FC=3.12)
427 (**Figure 6H**, **Figure S13**), but had reduced IFNG expression compared to TSCM and memory cells and similar
428 IL-2 and TNFα expression to TSCM cells, indicative of maintained functionality and potentially a
429 transitional phenotype. Importantly, these data support that this subset exhibits features of stemness as
430 well as polyfunctionality.

431 **TCF1$^+$TOX$^+$ T cells demonstrate tissue-specific phenotypes and localize to the islets in human T1D**

432 As single cell RNAseq analysis precludes the investigation of cell type localization, we performed
433 PhenoCycler analysis of pancreas and pLN from donor 6551 to examine the tissue localization of naïve-
434 like and terminal effector phenotypes in insulitis (**Figure 7A**). CD3$^+$ T cells were classified as TCF1$^+$TOX$^-$
435 (TCF1$^+$, naïve), TCF1$^-$TOX$^+$ (TOX$^+$, memory and exhausted), and TCF1$^+$TOX$^+$ (activated transitional and
436 effector) populations (**Figure 7B**). TCF1$^+$TOX$^+$ cells in the pancreas were found more often near or within
437 the islet boundary than TCF1$^+$ or TOX$^+$ cells, with TOX$^+$ cells more proximal than TCF1$^+$ (**Figure 7C**). In
438 accordance with our single cell analysis of CD8$^+$ T cells across tissues, we observed enhanced inhibitory
439 receptor expression (namely TOX, CD57, and PD-1) in TCF1$^+$TOX$^+$ and TOX$^+$ subsets in the pancreas relative
440 to the pLN (**Figure 7D-E**). Thus, these data indicate a spectrum of memory CD8$^+$ T cell phenotypes in the
441 pancreas, which include an activated TCF1$^+$TOX$^+$ population in close proximity to the islets. Akin to recent
442 reports in NOD mice that precursor diabetogenic T cells are primed and maintained as a self-renewing
443 pool in the pLN and seed terminally differentiated cells that expand in the islets[5], our data are indicative
444 of distinct tissue programs allowing for maintenance of CD8$^+$ T cell populations and prevention of
445 exhaustion in the pLN, as well as acquisition of further effector function in the pancreas during human
446 T1D.

447 **Discussion**

448 Despite tremendous progress in characterizing circulating immune cells in T1D, a critical gap in
449 knowledge remains as to alterations in tissue immune phenotypes. Large datasets derived from the
450 pancreas have given insight into disease-related changes in endocrine composition and function[90, 91],
451 as well as potential changes in immune:islet cell communication[90, 92], but have limited power to
452 examine immune cell phenotype. Datasets derived from secondary lymphoid organs in T1D are
453 lacking due to the limited availability of samples and, to date, paucity of receptor information[93]. This
454 study begins to address these gaps using complementary methods (i.e., CyTOF,
455 scRNAseq/TCRseq/CITEseq, spatial proteomics) to assess differences in T cell phenotypes and their
456 potential molecular underpinnings within the pLN and pancreas.

457 $CD8^+$ T cells are classically thought to be a major mediator of islet destruction in T1D, given
458 their abundance in the insulitic lesion[94] and cytolytic function[95-97]. Moreover, recent studies indicated
459 that $CD8^+$ T cells with a self-renewing phenotype may be important for T1D pathogenesis, as they are
460 elevated in peripheral blood, and autoreactive cells may be biased towards this phenotype[5, 14, 98]. Our
461 study shows that $CD8^+$ T cells expressing markers of a TSCM population (CD45RA, CCR7, CXCR3, CD27,
462 CD28) are increased in T1D pLN. TSCM cells play an important role in memory maintenance and in
463 generating rapidly responding effector cells[99]. It has been shown that serum concentrations of
464 cytokines that promote TSCM development, notably IL-15, are elevated in T1D patients[100, 101].
465 Moreover, circulating islet antigen-reactive T cells from T1D donors have been shown to possess
466 stem-like features[14]. Enhanced capacity for self-renewal could be clinically detrimental, as multiple
467 therapeutic avenues (e.g., teplizumab, anti-thymocyte globulin [ATG]) have converged on a signature
468 of CD8 T cell exhaustion in therapeutic responders[13, 102]. Our study provides further support for the
469 relevance of this pathway, as IREA analysis revealed an enrichment of IL-15-induced genes across the

470 trajectory of CD8$^+$ T cell differentiation in T1D. Interestingly, pathway analysis of naïve cells indicated
471 an enrichment of autophagy and mitophagy in cells from T1D pLN. IL-15 has recently been shown to
472 enable sustained autophagy during activation as compared to inflammatory cytokines[103], potentially
473 better enabling maintenance of memory populations. We also observed an increase in cytokine
474 signaling and upregulation of the anti-apoptotic factor *BCL2,* which, coupled with the downregulation
475 of multiple exhaustion-associated genes in this cluster in T1D, could suggest that CD8 T cells favor a
476 progenitor exhausted phenotype rather than a terminal exhaustion phenotype in T1D[62]. Further
477 studies are needed to connect IL-15 signaling in T1D to autoreactive T cell stemness and progenitor
478 exhausted phenotypes and to investigate if inhibiting this pathway may aid in establishing durable
479 tolerance. Notably, baricitinib, an inhibitor of Janus Kinase (JAK) 1/2 signaling and thus, common
480 gamma chain cytokine signaling (including IL-15), has recently demonstrated efficacy in preserving β-
481 cell function in recent-onset T1D donors[104]. Interestingly, we observed reduced expression of *IL7R*
482 and *IL2RG* in effector cells derived from the recent-onset T1D pancreas relative to those from paired
483 pLN, indicating that in the pancreas microenvironment, these cells may be more reliant on IL-15 and
484 other effector cytokines, such as IL-21, than IL-2 or IL-7. It remains to be seen whether baricitinib
485 alone could aid in targeting the autoreactive T cell reservoir or if combinatorial therapy will be
486 necessary with T cell exhaustion-inducing therapeutics, such as teplizumab.

487 Limitations of the study include donor heterogeneity and limited sample size due to the rarity
488 of study tissues. Notably, we were unable to obtain sufficient immune cell numbers from control
489 pancreatic slices to compare immune phenotypes between T1D and ND donors, and our small
490 sampling size from pancreatic slices likely is not representative of the full complement of immune cell
491 phenotypes in the target organ. Our lab is currently utilizing spatial transcriptomic[105] and proteomic
492 technologies to assess this without the need for immune cell isolation. Moreover, T1D is a

493 heterogeneous disease, and it is possible that immune phenotypes identified through our studies
494 may differ across different age or ancestry groups, which we were not powered to assess. Indeed,
495 though great strides are being made in investigating the genetic drivers of T1D in populations with
496 diverse genetic ancestry[106-108], there are still many knowledge gaps regarding the importance of
497 known genetic risk loci across groups traditionally underrepresented in biomedical research. Despite
498 this, we believe that the information that we have provided using paired phenotype and receptor
499 information for these subsets can be used by the field to identify CDR3 motifs of further interest.

500 As it stands, known TCR sequences that correspond to autoreactive T cell specificity are rare[78].
501 Moreover, matching sequences to those in curated databases such as the Manually curated database
502 of Pathology Associated Sequences (McPAS)[109] and Immune Epitope Database (IEDB)[110] introduces a
503 bias toward known specificities and epitopes of interest. Indeed, we were unable to confidently
504 identify a priori T1D antigen autoreactive cells using pMHC dextramer reagents. This could reflect low
505 sampling (10,000 cells per donor), incomplete knowledge of antigen reactivity, and/or individual
506 heterogeneity in autoantigen reactivity. However, utilizing a curated list of experimentally validated
507 T1D clones, we identified 11 putative T1D clones in the pLN based on a priori knowledge.
508 Nevertheless, there is a need to apply new analytical strategies to identify similarities in TCR sequence
509 and transcriptomic features that may indicate a common antigen specificity[111]. We utilized one such
510 tool, CoNGA[31], to examine joint gene expression and receptor features in T1D. This analysis revealed
511 a T1D-associated enrichment of a TCR cluster comprised of diverse naive $CD8^+$ T cells that display
512 features of prior activation (i.e., *KLRK1*, *HCST*, low *CXCR3*), further supporting our gene expression
513 and proteomic data. The feature of low AF4 within this cluster supports previous data wherein
514 autoreactive T cells were found to possess more hydrophobic residues[112], including within
515 autoreactive receptors detected in the pancreas[79]. Moreover, in T1D pLN we also found enrichment

516 of a more terminally differentiated cluster of CD8$^+$ T cells, which displayed expression of cytotoxicity-
517 related genes, *CXCR3*, and memory/exhaustion-related gene *TOX*, while retaining some *TCF7*
518 expression. Though infrequent, we postulated that this population may represent a transitional
519 memory phenotype that is poised to infiltrate the pancreas, as supported by the presence of an
520 expanded putative autoreactive clone in this population in a new-onset T1D donor.

521 We utilized paired pLN and pancreas T cell data to investigate phenotypes of shared
522 populations and to interrogate whether local expansion of T cells occurred in fresh pancreatic slices.
523 We identified the most abundant shared populations to be effector CD8$^+$ T cells, which were the most
524 clonally expanded populations. Moreover, we noted CD8$^+$ T cells, as a whole, had reduced expression
525 of genes involved in promoting stem-like/naïve phenotypes (*LEF1, SELL*) in pancreas compared to
526 pLN. This could, in part, be driven by the local inflammatory milieu. Indeed, we observed enrichment
527 of multiple inflammatory cytokine signaling pathways, namely IL-6 and TNFα, in pancreas relative to
528 pLN T cells, while we observed upregulation of Myc, mTORC1, and Wnt signaling pathways in pLN
529 relative to pancreas T cells. While sharing of TCR clones was limited between donors and difficult to
530 detect due to the sparsity of single cell data, we were able to detect intra-donor sharing of clones
531 across tissues and between clusters. Donor 6551, a 20-year-old donor with 0.58 years T1D duration,
532 particularly notable for insulitis severity, possessed expanded CD8$^+$ Teff clones that were shared
533 between tissues and between clusters. In the longer duration (4 years) donor with less insulitis (6536),
534 we were able to detect sharing of only one effector CD8$^+$ clone across clusters and one CD4$^+$ clone
535 across tissues.

536 Using multiplex spatial proteomic profiling, we were able to show that in the same T1D donor
537 with marked insulitis, case 6551, TCF1 and TOX expressing T cell populations can be found in pLN and
538 pancreas. Importantly, we found that TCF1$^+$TOX$^+$ cells possess a more terminal effector phenotype in

539 the pancreas and can be found proximal to the islets. We also found by flow cytometry that pLN naive
540 CXCR3^{+} T cells have similar expression of transcription factors TCF1 and TOX to TSCM cells, and
541 produce similar levels of proinflammatory cytokines upon activation. Akin to human peripheral blood
542 data, we noted that TCF1-expressing populations in the pLN tended to express less PD-1 and more
543 CD127[113] and CD5[114], indicative of early differentiation stage and activation potential. In accordance
544 with murine studies[5], these data collectively support that T cell clones are supplied from the pLN and
545 adopt a more effector and terminally differentiated phenotype in the pancreas during human T1D
546 development. Previously, our lab reported increased circulating CXCR3^{lo}CD8^{+} T cells in T1D[75] following
547 phenotyping of a cohort of over 824 cross-sectional peripheral blood samples. The present study
548 supports a role for these cells in the draining lymph node: a small set of related terminal effector
549 CXCR3-expressing cells could be found in the pLN and a larger fraction in the target organ, suggesting
550 that these cells share some features of stemness (TCF1 expression) and are more polyfunctional as
551 compared to naïve cells. Identifying subsets of interest that are relevant in both peripheral blood and
552 the target organ could aid in efforts to selectively inhibit autoreactivity and monitor outcomes.
553 Importantly, combination CXCR3 antagonism with ACT-777991 and α-CD3 treatment leads to disease
554 remission in the NOD mouse[115], and first-in-human trials in healthy adults have shown this compound
555 to be tolerable[116]. Thus, combinatorial strategies to induce tolerogenic phenotypes while targeting
556 pathways relevant to tissue immune phenotypes may represent an avenue to achieve durable
557 tolerance. Taken together, our studies indicate that memory and effector T cell programs in T1D are
558 maintained in the pLN and enhanced locally in the pancreas, likely driven by aberrant regulation of
559 cytokine signaling and impacted by genotype at T1D risk loci. Future directions validating the
560 functionality of clones identified herein and investigating the cellular interactions of CXCR3^{+}CD8^{+} T

561 cells across the differentiation trajectory will inform the development of therapeutics to modulate

562 them, providing novel avenues to delay or prevent T1D progression.

563 **Author Contributions**

564 LDP: Designing research studies, conducting experiments, acquiring data, analyzing data, writing the
565 manuscript (original draft), funding acquisition

566 HRS: Conducting experiments, acquiring data, writing the manuscript (reviewing and editing)

567 JS: Conducting experiments, acquiring data, analyzing data, writing the manuscript (original draft)

568 ALP: Writing the manuscript (reviewing and editing)

569 RLB: Acquiring data, writing the manuscript (reviewing and editing)

570 CHW: Writing the manuscript (reviewing and editing)

571 MAA: Writing the manuscript (reviewing and editing), funding acquisition

572 RB: Analyzing data, writing the manuscript (reviewing and editing), interpreting data

573 MAB: Designing research studies, interpreting data, writing the manuscript (reviewing and editing),
574 project oversight

575 TMB: Designing research studies, interpreting data, writing the manuscript (reviewing and editing),
576 funding acquisition, project oversight

577 **Acknowledgments**

578 We thank the nPOD donor families for their important contributions to this research. We also thank
579 the nPOD Organ Processing and Pathology Core (OPPC) team, namely Irina Kusmartseva, Helmut
580 Hiller, and Maria Beery, for their efforts in case acquisition, processing, and distribution.

581 **Funding**

582 This research was conducted with grant support from the National Institutes of Health (NIH) P01
583 AI042288 to TMB, F31 DK129004 to LDP, as well as from the American Diabetes Association (ADA) 11-

584 23-PDF-78 to LDP, and The Leona M. and Harry B. Helmsley Charitable Trust (Grant # 2301-06562 to
585 TMB). This research was also performed with the support of the Network for Pancreatic Organ donors
586 with Diabetes (nPOD; RRID:SCR_014641), a collaborative type 1 diabetes research project supported
587 by Breakthrough T1D and The Leona M. & Harry B. Helmsley Charitable Trust (Grant#3-SRA-2023-
588 1417-S-B). The content and views expressed are the responsibility of the authors and do not
589 necessarily reflect the official view of nPOD. Organ Procurement Organizations (OPO) partnering with
590 nPOD to provide research resources are listed at **https://npod.org/for-partners/npod-partners/**.

591

592

593

References

1. Onengut-Gumuscu, S., et al., *Fine mapping of type 1 diabetes susceptibility loci and evidence for colocalization of causal variants with lymphoid gene enhancers.* Nat Genet, 2015. **47**(4): p. 381-6.
2. Wan, X., et al., *Pancreatic islets communicate with lymphoid tissues via exocytosis of insulin peptides.* Nature, 2018. **560**(7716): p. 107-111.
3. Turley, S., et al., *Physiological beta cell death triggers priming of self-reactive T cells by dendritic cells in a type-1 diabetes model.* J Exp Med, 2003. **198**(10): p. 1527-37.
4. Marrero, I., et al., *High-throughput sequencing reveals restricted TCR Vbeta usage and public TCRbeta clonotypes among pancreatic lymph node memory CD4(+) T cells and their involvement in autoimmune diabetes.* Mol Immunol, 2016. **74**: p. 82-95.
5. Gearty, S.V., et al., *An autoimmune stem-like CD8 T cell population drives type 1 diabetes.* Nature, 2022. **602**(7895): p. 156-161.
6. Vecchione, A., et al., *Reduced Follicular Regulatory T Cells in Spleen and Pancreatic Lymph Nodes of Patients With Type 1 Diabetes.* Diabetes, 2021. **70**(12): p. 2892-2902.
7. Ferraro, A., et al., *Expansion of Th17 cells and functional defects in T regulatory cells are key features of the pancreatic lymph nodes in patients with type 1 diabetes.* Diabetes, 2011. **60**(11): p. 2903-13.
8. Putnam, A.L., et al., *Expansion of human regulatory T-cells from patients with type 1 diabetes.* Diabetes, 2009. **58**(3): p. 652-62.
9. McClymont, S.A., et al., *Plasticity of human regulatory T cells in healthy subjects and patients with type 1 diabetes.* J Immunol, 2011. **186**(7): p. 3918-26.
10. Sebastiani, G., et al., *Regulatory T-cells from pancreatic lymphnodes of patients with type-1 diabetes express increased levels of microRNA miR-125a-5p that limits CCR2 expression.* Sci Rep, 2017. **7**(1): p. 6897.
11. Arif, S., et al., *Erratum. Blood and Islet Phenotypes Indicate Immunological Heterogeneity in Type 1 Diabetes. Diabetes 2014;63:3835-3845.* Diabetes, 2015. **64**(9): p. 3334.
12. Diggins, K.E., et al., *Exhausted-like CD8+ T cell phenotypes linked to C-peptide preservation in alefacept-treated T1D subjects.* JCI Insight, 2021. **6**(3).
13. Long, S.A., et al., *Partial exhaustion of CD8 T cells and clinical response to teplizumab in new-onset type 1 diabetes.* Science Immunology, 2016. **1**(5).
14. Abdelsamed, H.A., et al., *Beta cell-specific CD8+ T cells maintain stem cell memory-associated epigenetic programs during type 1 diabetes.* Nature Immunology, 2020. **21**(5).
15. Balmas, E., et al., *Islet-autoreactive CD4+ T cells are linked with response to alefacept in type 1 diabetes.* JCI Insight, 2023. **8**(21).
16. Seay, H.R., et al., *Tissue distribution and clonal diversity of the T and B cell repertoire in type 1 diabetes.* JCI Insight, 2016. **1**(20): p. e88242.
17. Campbell-Thompson, M., et al., *Network for Pancreatic Organ Donors with Diabetes (nPOD): developing a tissue biobank for type 1 diabetes.* Diabetes Metab Res Rev, 2012. **28**(7): p. 608-17.
18. Drotar, D.M., et al., *Impaired islet function and normal exocrine enzyme secretion occur with low inter-regional variation in type 1 diabetes.* Cell Rep, 2024. **43**(6): p. 114346.
19. Shapiro, M.R., et al., *Human immune phenotyping reveals accelerated aging in type 1 diabetes.* JCI Insight, 2023.
20. Subrahmanyam, P.B. and H.T. Maecker, *CyTOF Measurement of Immunocompetence Across Major Immune Cell Types.* Curr Protoc Cytom, 2017. **82**: p. 9 54 1-9 54 12.

639 21. Crowell, H.L., et al., *An R-based reproducible and user-friendly preprocessing pipeline for CyTOF*
640 *data.* F1000Res, 2020. **9**: p. 1263.
641 22. Hahne, F., et al., *flowCore: a Bioconductor package for high throughput flow cytometry.* BMC
642 Bioinformatics, 2009. **10**: p. 106.
643 23. Phipson, B., et al., *propeller: testing for differences in cell type proportions in single cell data.*
644 Bioinformatics, 2022. **38**(20): p. 4720-4726.
645 24. McGinnis, C.S., L.M. Murrow, and Z.J. Gartner, *DoubletFinder: Doublet Detection in Single-Cell*
646 *RNA Sequencing Data Using Artificial Nearest Neighbors.* Cell Syst, 2019. **8**(4): p. 329-337 e4.
647 25. Mule, M.P., A.J. Martins, and J.S. Tsang, *Normalizing and denoising protein expression data from*
648 *droplet-based single cell profiling.* Nat Commun, 2022. **13**(1): p. 2099.
649 26. Hao, Y., et al., *Integrated analysis of multimodal single-cell data.* Cell, 2021. **184**(13): p. 3573-
650 3587 e29.
651 27. Borcherding, N., N.L. Bormann, and G. Kraus, *scRepertoire: An R-based toolkit for single-cell*
652 *immune receptor analysis.* F1000Res, 2020. **9**: p. 47.
653 28. Finak, G., et al., *MAST: a flexible statistical framework for assessing transcriptional changes and*
654 *characterizing heterogeneity in single-cell RNA sequencing data.* Genome Biol, 2015. **16**: p. 278.
655 29. Yu, G. and Q.Y. He, *ReactomePA: an R/Bioconductor package for reactome pathway analysis and*
656 *visualization.* Mol Biosyst, 2016. **12**(2): p. 477-9.
657 30. Borcherding, N., et al., *Mapping the immune environment in clear cell renal carcinoma by single-*
658 *cell genomics.* Commun Biol, 2021. **4**(1): p. 122.
659 31. Schattgen, S.A., et al., *Integrating T cell receptor sequences and transcriptional profiles by*
660 *clonotype neighbor graph analysis (CoNGA).* Nat Biotechnol, 2022. **40**(1): p. 54-63.
661 32. Bankhead, P., et al., *QuPath: Open source software for digital pathology image analysis.* Sci Rep,
662 2017. **7**(1): p. 16878.
663 33. Goldsborough, T., et al. *InstanSeg: an embedding-based instance segmentation algorithm*
664 *optimized for accurate, efficient and portable cell segmentation*. 2024. arXiv:2408.15954 DOI:
665 10.48550/arXiv.2408.15954.
666 34. Smith, J.A., et al., *Protocol for processing and analyzing multiplexed images improves lymphatic*
667 *cell identification and spatial architecture in human tissue.* STAR Protoc, 2025. **6**(3): p. 103976.
668 35. Perry, D.J., et al., *A genomic data archive from the Network for Pancreatic Organ donors with*
669 *Diabetes.* Sci Data, 2023. **10**(1): p. 323.
670 36. Wiedeman, A.E., et al., *Autoreactive CD8+ T cell exhaustion distinguishes subjects with slow type*
671 *1 diabetes progression.* Journal of Clinical Investigation, 2020. **130**(1).
672 37. Laban, S., et al., *Heterogeneity of circulating CD8 T-cells specific to islet, neo-antigen and virus in*
673 *patients with type 1 diabetes mellitus.* PLoS ONE, 2018. **13**(8).
674 38. Uno, S., et al., *Expression of chemokines, CXC chemokine ligand 10 (CXCL10) and CXCR3 in the*
675 *inflamed islets of patients with recent-onset autoimmune type 1 diabetes.* Endocr J, 2010.
676 **57**(11): p. 991-6.
677 39. Cao, C., X. Fu, and X. Wang, *Case Report: A novel mutation in TNFAIP3 in a patient with type 1*
678 *diabetes mellitus and haploinsufficiency of A20.* Front Endocrinol (Lausanne), 2023. **14**: p.
679 1131437.
680 40. Meixner, A., et al., *JunD regulates lymphocyte proliferation and T helper cell cytokine expression.*
681 EMBO J, 2004. **23**(6): p. 1325-35.
682 41. Bedford, J.G., et al., *Rapid interferon independent expression of IFITM3 following T cell activation*
683 *protects cells from influenza virus infection.* PLoS One, 2019. **14**(1): p. e0210132.
684 42. Merkley, S.D., et al., *Modulating T Cell Responses via Autophagy: The Intrinsic Influence*
685 *Controlling the Function of Both Antigen-Presenting Cells and T Cells.* Front Immunol, 2018. **9**: p.
686 2914.

687 43. Kumar, A.V., J. Mills, and L.R. Lapierre, *Selective Autophagy Receptor p62/SQSTM1, a Pivotal*
688 *Player in Stress and Aging.* Front Cell Dev Biol, 2022. **10**: p. 793328.
689 44. Zheng, M.M., et al., *IMPDH inhibitors upregulate PD-L1 in cancer cells without impairing immune*
690 *checkpoint inhibitor efficacy.* Acta Pharmacol Sin, 2025. **46**(4): p. 1058-1067.
691 45. Baldwin, J.G., C.R.F. Silveira, and L. Gattinoni, *Restoring the supply lines: removing roadblocks to*
692 *fatty acid uptake enhances T cell-driven cancer fight.* Signal Transduct Target Ther, 2025. **10**(1):
693 p. 53.
694 46. Kolumam, G.A., et al., *Type I interferons act directly on CD8 T cells to allow clonal expansion and*
695 *memory formation in response to viral infection.* J Exp Med, 2005. **202**(5): p. 637-50.
696 47. Ng, D., et al., *A Lymphotoxin/Type I IFN Axis Programs CD8*

697 *T Cells To Infiltrate a Self-Tissue and Propagate Immunopathology.* Journal of Immunology, 2015.
698 **195**(10): p. 4650-4659.
699 48. Carow, B. and M.E. Rottenberg, *SOCS3, a Major Regulator of Infection and Inflammation.* Front
700 Immunol, 2014. **5**: p. 58.
701 49. Joosten, L.A., et al., *IL-32, a proinflammatory cytokine in rheumatoid arthritis.* Proc Natl Acad Sci
702 U S A, 2006. **103**(9): p. 3298-303.
703 50. Ciecko, A.E., et al., *Interleukin-27 Is Essential for Type 1 Diabetes Development and Sjogren*
704 *Syndrome-like Inflammation.* Cell Rep, 2019. **29**(10): p. 3073-3086 e5.
705 51. Jaiswal, H., et al., *The NF-kappaB regulator Bcl-3 restricts terminal differentiation and promotes*
706 *memory cell formation of CD8+ T cells during viral infection.* PLoS Pathog, 2021. **17**(1): p.
707 e1009249.
708 52. Sun, Q., et al., *BCL6 promotes a stem-like CD8(+) T cell program in cancer via antagonizing*
709 *BLIMP1.* Sci Immunol, 2023. **8**(88): p. eadh1306.
710 53. Seo, H., et al., *BATF and IRF4 cooperate to counter exhaustion in tumor-infiltrating CAR T cells.*
711 Nat Immunol, 2021. **22**(8): p. 983-995.
712 54. Ilangumaran, S., D. Bobbala, and S. Ramanathan, *SOCS1: Regulator of T Cells in Autoimmunity*
713 *and Cancer.* Curr Top Microbiol Immunol, 2017. **410**: p. 159-189.
714 55. Lu, D., et al., *The phosphatase PAC1 acts as a T cell suppressor and attenuates host antitumor*
715 *immunity.* Nature Immunology, 2020. **21**(3): p. 287-+.
716 56. Srirat, T., et al., *NR4a1/2 deletion promotes accumulation of TCF1(+) stem-like precursors of*
717 *exhausted CD8(+) T cells in the tumor microenvironment.* Cell Rep, 2024. **43**(3): p. 113898.
718 57. Yang, H., et al., *Stress-glucocorticoid-TSC22D3 axis compromises therapy-induced antitumor*
719 *immunity.* Nat Med, 2019. **25**(9): p. 1428-1441.
720 58. Cantor, J., et al., *Loss of T cell CD98hc specifically ablates T cell clonal expansion and protects*
721 *from autoimmunity.* Journal of Immunology, 2011. **186**.
722 59. Ng, S.S., et al., *The NK cell granule protein NKG7 regulates cytotoxic granule exocytosis and*
723 *inflammation.* Nat Immunol, 2020. **21**(10): p. 1205-1218.
724 60. Li, D., et al., *Intermediate Filament (IF) Protein Vimentin Regulates T Cell Mediated Immune*
725 *Response in Gvhd.* Blood, 2015. **126**(23).
726 61. Kollis, P.M., et al., *Characterising Distinct Migratory Profiles of Infiltrating T-Cell Subsets in*
727 *Human Glioblastoma.* Front Immunol, 2022. **13**: p. 850226.
728 62. Nagasaki, J., et al., *T cells with high BCL-2 expression induced by venetoclax impact anti-leukemic*
729 *immunity "graft-versus-leukemia effects".* Blood Cancer Journal, 2024. **14**(1).
730 63. Kurtulus, S., et al., *Bcl-2 allows effector and memory CD8+ T cells to tolerate higher expression of*
731 *Bim.* J Immunol, 2011. **186**(10): p. 5729-37.
732 64. Cao, C., et al., *CXCR4 orchestrates the TOX-programmed exhausted phenotype of CD8(+) T cells*
733 *via JAK2/STAT3 pathway.* Cell Genom, 2024. **4**(10): p. 100659.

65. Donato, R., *Functional roles of S100 proteins, calcium-binding proteins of the EF-hand type.* Biochim Biophys Acta, 1999. **1450**(3): p. 191-231.
66. Ganes, S. and V. Fensterl, *Interferon-induced Ifit proteins: Their role in viral pathogenesis.* Cytokine, 2015. **76**(1): p. 64-64.
67. Su, L., et al., *HMGN2, a new anti-tumor effector molecule of CD8(+) T cells.* Mol Cancer, 2014. **13**: p. 178.
68. Wang, Y., et al., *HLA-DR Expression Level in CD8(+) T Cells Correlates With the Severity of Children With Acute Infectious Mononucleosis.* Front Immunol, 2021. **12**: p. 753290.
69. Lyngstadaas, A.V., et al., *Pro-Resolving Mediator Annexin A1 Regulates Intracellular Ca(2+) and Mucin Secretion in Cultured Goblet Cells Suggesting a New Use in Inflammatory Conjunctival Diseases.* Front Immunol, 2021. **12**: p. 618653.
70. Momenilandi, M., et al., *FLT3L governs the development of partially overlapping hematopoietic lineages in humans and mice.* Cell, 2024. **187**(11): p. 2817-2837 e31.
71. Brault, L., et al., *PIM kinases are progression markers and emerging therapeutic targets in diffuse large B-cell lymphoma.* Br J Cancer, 2012. **107**(3): p. 491-500.
72. Cui, A., et al., *Dictionary of immune responses to cytokines at single-cell resolution.* Nature, 2024. **625**(7994).
73. Lee, J., et al., *IL-15 promotes self-renewal of progenitor exhausted CD8 T cells during persistent antigenic stimulation.* Front Immunol, 2023. **14**: p. 1117092.
74. Klebanoff, C.A., et al., *IL-15 enhances the in vivo antitumor activity of tumor-reactive CD8+ T cells.* Proc Natl Acad Sci U S A, 2004. **101**(7): p. 1969-74.
75. Shapiro, M.R., et al., *Human immune phenotyping reveals accelerated aging in type 1 diabetes.* JCI Insight, 2023. **8**(17).
76. Ogasawara, K., et al., *NKG2D blockade prevents autoimmune diabetes in NOD mice.* Immunity, 2004. **20**(6): p. 757-67.
77. Li, S., et al., *DAP10 integration in CAR-T cells enhances the killing of heterogeneous tumors by harnessing endogenous NKG2D.* Mol Ther Oncolytics, 2022. **26**: p. 15-26.
78. Mitchell, A.M., et al., *Tracking DNA-based antigen-specific T cell receptors during progression to type 1 diabetes.* Sci Adv, 2023. **9**(49): p. eadj6975.
79. Linsley, P.S., et al., *Germline-like TCR-α chains shared between autoreactive T cells in blood and pancreas.* Nature Communications, 2024. **15**(1).
80. Anderson, A.M., et al., *Human islet T cells are highly reactive to preproinsulin in type 1 diabetes.* Proceedings of the National Academy of Sciences of the United States of America, 2021. **118**(41).
81. Liang, T., et al., *Ex vivo human pancreatic slice preparations offer a valuable model for studying pancreatic exocrine biology.* J Biol Chem, 2017. **292**(14): p. 5957-5969.
82. Marciniak, A., et al., *Using pancreas tissue slices for in situ studies of islet of Langerhans and acinar cell biology.* Nat Protoc, 2014. **9**(12): p. 2809-22.
83. Huber, M.K., et al., *Beta Cell Dysfunction Occurs Independently of Insulitis in Type 1 Diabetes Pathogenesis.* bioRxiv, 2024.
84. Sutherland, C.L., et al., *UL16-binding proteins, novel MHC class I-related proteins, bind to NKG2D and activate multiple signaling pathways in primary NK cells.* J Immunol, 2002. **168**(2): p. 671-9.
85. Kirkham, C.L. and J.R. Carlyle, *Complexity and Diversity of the NKR-P1:Clr (Klrb1:Clec2) Recognition Systems.* Front Immunol, 2014. **5**: p. 214.
86. Yoon, S.H., et al., *Selective addition of CXCR3(+) CCR4(-) CD4(+) Th1 cells enhances generation of cytotoxic T cells by dendritic cells in vitro.* Exp Mol Med, 2009. **41**(3): p. 161-70.
87. Wang, Y., et al., *Characteristics of premanufacture CD8(+)T cells determine CAR-T efficacy in patients with diffuse large B-cell lymphoma.* Signal Transduct Target Ther, 2023. **8**(1): p. 409.

88. Zhao, Y., et al., *An integrative analysis of the single-cell transcriptome identifies DUSP4 as an exhaustion-associated gene in tumor-infiltrating CD8+T cells.* Functional & Integrative Genomics, 2023. **23**(2).
89. Patterson, A.R., et al., *Gimap5-dependent inactivation of GSK3β is required for CD4 T cell homeostasis and prevention of immune pathology.* Journal of Immunology, 2018. **200**(1).
90. Wang, Y.J., et al., *Multiplexed In Situ Imaging Mass Cytometry Analysis of the Human Endocrine Pancreas and Immune System in Type 1 Diabetes.* Cell Metab, 2019. **29**(3): p. 769-783 e4.
91. Ackermann, A.M., et al., *Integration of ATAC-seq and RNA-seq identifies human alpha cell and beta cell signature genes.* Mol Metab, 2016. **5**(3): p. 233-244.
92. Fasolino, M., et al., *Single-cell multi-omics analysis of human pancreatic islets reveals novel cellular states in type 1 diabetes.* Nat Metab, 2022. **4**(2): p. 284-299.
93. Golden, G.J., et al., *Immune perturbations in human pancreas lymphatic tissues prior to and after type 1 diabetes onset.* bioRxiv, 2024.
94. Coppieters, K.T., et al., *Demonstration of islet-autoreactive CD8 T cells in insulitic lesions from recent onset and long-term type 1 diabetes patients.* J Exp Med, 2012. **209**(1): p. 51-60.
95. Dean, J.W., et al., *Innate inflammation drives NK cell activation to impair Treg activity.* J Autoimmun, 2020. **108**: p. 102417.
96. Peters, L.D., et al., *Modeling cell-mediated immunity in human type 1 diabetes by engineering autoreactive CD8(+) T cells.* Front Immunol, 2023. **14**: p. 1142648.
97. Newby, B.N., et al., *Type 1 interferons potentiate human cd8+ t-cell cytotoxicity through a stat4- and granzyme b-dependent pathway.* Diabetes, 2017. **66**(12).
98. Vignali, D., et al., *Detection and characterization of CD8+ autoreactive memory Stem T cells in patients with type 1 diabetes.* Diabetes, 2018. **67**(5).
99. Wang, Y.T., et al., *Stem cell-like memory T cells: The generation and application.* Journal of Leukocyte Biology, 2021. **110**(6): p. 1209-1223.
100. Chen, J., et al., *Insulin-dependent diabetes induced by pancreatic beta cell expression of IL-15 and IL-15Rα.* Proceedings of the National Academy of Sciences of the United States of America, 2013. **110**(33): p. 13534-13539.
101. Kuczynski, S., et al., *IL-15 is elevated in serum patients with type 1 diabetes mellitus.* Diabetes Research and Clinical Practice, 2005. **69**(3): p. 231-236.
102. Jacobsen, L.M., et al., *Responders to low-dose ATG induce CD4+ T cell exhaustion in type 1 diabetes.* JCI Insight, 2023. **8**(16).
103. Sinclair, L.V., et al., *Autophagy repression by antigen and cytokines shapes mitochondrial, migration and effector machinery in CD8 T cells.* Nat Immunol, 2025. **26**(3): p. 429-443.
104. Waibel, M., et al., *Baricitinib and beta-Cell Function in Patients with New-Onset Type 1 Diabetes.* N Engl J Med, 2023. **389**(23): p. 2140-2150.
105. Medina-Serpas, M.A., et al., *Spatial transcriptomics from pancreas and local draining lymph node tissue reveals a lymphotoxin-beta signature in human type 1 diabetes.* Cell Rep, 2026. **45**(4): p. 117144.
106. Perry, D.J., et al., *A genomic data archive from the Network for Pancreatic Organ donors with Diabetes.* Scientific Data, 2023. **10**(1): p. 323.
107. Robertson, C.C., et al., *Fine-mapping, trans-ancestral and genomic analyses identify causal variants, cells, genes and drug targets for type 1 diabetes.* Nat Genet, 2021. **53**(7): p. 962-971.
108. Perry, D.J., et al., *Application of a Genetic Risk Score to Racially Diverse Type 1 Diabetes Populations Demonstrates the Need for Diversity in Risk-Modeling.* Sci Rep, 2018. **8**(1): p. 4529.
109. Tickotsky, N., et al., *McPAS-TCR: a manually curated catalogue of pathology-associated T cell receptor sequences.* Bioinformatics, 2017. **33**(18): p. 2924-2929.

829 110. Vita, R., et al., *The Immune Epitope Database (IEDB): 2024 update.* Nucleic Acids Res, 2025.
830 **53**(D1): p. D436-D443.
831 111. Gao, S., et al., *Single-cell RNA sequencing coupled to TCR profiling of large granular lymphocyte*
832 *leukemia T cells.* Nat Commun, 2022. **13**(1): p. 1982.
833 112. Stadinski, B.D., et al., *Hydrophobic CDR3 residues promote the development of self-reactive T*
834 *cells.* Nat Immunol, 2016. **17**(8): p. 946-55.
835 113. Kratchmarov, R., A.M. Magun, and S.L. Reiner, *TCF1 expression marks self-renewing human*
836 *CD8(+) T cells.* Blood Adv, 2018. **2**(14): p. 1685-1690.
837 114. Kim, Y.J., et al., *CD5 Expression Dynamically Changes During the Differentiation of Human CD8(+)*
838 *T Cells Predicting Clinical Response to Immunotherapy.* Immune Netw, 2023. **23**(4): p. e35.
839 115. Christen, U., et al., *Combination treatment of a novel CXCR3 antagonist ACT-777991 with an*
840 *anti-CD3 antibody synergistically increases persistent remission in experimental models of type 1*
841 *diabetes.* Clin Exp Immunol, 2023. **214**(2): p. 131-143.
842 116. Boof, M.L., et al., *Pharmacokinetics, pharmacodynamics and safety of the novel C-X-C chemokine*
843 *receptor 3 antagonist ACT-777991: Results from the first-in-human study in healthy adults.* Br J
844 Clin Pharmacol, 2024. **90**(2): p. 588-599.

845

846

847 **Tables**

848

849 Table 1. Sequences of shared clones across pLN and pancreas slices.

Tissue(s)	Donor	Cluster number	Cluster phenotype	CDR3 sequence (amino acid)	CDR3 sequence (nt)	TCR gene usage	n
pLN, slice	6536	5,9	eTreg, ICOS^{hi} TCM	CAASIGFGNVLHC_CSSKKGLDEQFF	TGTGCAGCAAGTATAGGCTTTGGGAATGTGCTGCATTGC_TGCAGTTCCAAGAAGGGGTTGGATGAGCAGTTCTTC	TRAV13-1/TRAJ35 TRBV20-1/TRBJ2-1	4
pLN	6551	0,2	CD8 Teff, CD8 CTL	CAVDSGGGADGLTF_CASSPAGAGYEQYF	TGTGCTGTCGATTCAGGAGGAGGTGCTGACGGACTCACCTTT_TGCGCCAGCAGCCCTGCGGGGGCCGGCTACGAGCAGTACTTC TGTGCTGTGGATTCAGGAGGAGGTGCTGACGGACTCACCTTT_TGCGCCAGCAGCCCGGCCGGTGCGGGGTACGAGCAGTACTTC TGTGCTGTCGATTCAGGAGGAGGTGCTGACGGACTCACCTTT_TGCGCCAGCAGCCCTGCGGGGGCCGGCTACGAGCAGTACTTC	TRAV22/TRAJ45 TRBV4-3/TRBJ2-7	4
pLN	6551	0,2	CD8 Teff, CD8 CTL	CAMRGPFRAGANNLFF_CSARGGPVSNEQFF	TGTGCAATGAGAGGCCCCTTTCGAGCTGGGGCAAACAACCTCTTCTTT_TGCAGTGCTAGGGGTGGACCCGTCTCCAATGAGCAGTTCTTC	TRAV14/DV4/TRAJ36 TRBV20-1/TRBJ2-1	3
pLN, slice	6551	0,2	CD8 Teff, CD8 CTL	CASKTGANNLFF_CASAPGQGSEQLFF	TGTGCTTCTAAAACTGGGGCAAACAACCTCTTCTTT_TGTGCCAGTGCCCCGGGACAGGGCTCCGAGCAACTGTTTTTT	TRAV16/TRAJ36 TRBV19/TRBJ1-4	3
pLN	6551	0,2	CD8 Teff, CD8 CTL	CAVKDNARLMF_CASSSGEAGTNSPLHF	TGTGCTGTGAAAGACAATGCCAGACTCATGTTT_TGTGCCAGCAGCTCAGGGGAGGCAGGAACTAATTCACCCCTCCACTTT	TRAV1-2/TRAJ31 TRBV7-8/TRBJ1-6	3
pLN	6536	0,2	CD8 Teff, CD8 CTL	CAVRSPSLMDSNYQLIW_CASCRTGNYEQYF	TGCGCTGTGAGATCCCCTTCGTTAATGGATAGCAACTATCAGTTAATCTGG_TGTGCCAGCTGCCGGACAGGCAACTACGAGCAGTACTTC	TRAV1-1/TRAJ33 TRBV6-5/TRBJ2-7	3

850

851

852

853 **Figures Legends**

854

855 **Figure 1. Differential abundance of CXCR3^{lo} naïve CD8 T cells in T1D pLN.** A) Experimental workflow
856 involving processing of pancreatic lymph node (pLN), staining for lineage, phenotypic, and quality
857 control (QC) markers, and data collection on a mass cytometer. After data acquisition, normalization
858 of channels to internal bead controls was performed using the premessa[21] package, and any
859 confounding effects of batch or donor age on cluster composition were accounted for in analysis
860 through incorporation as covariates in a linear model. B) UMAP of subclustered CD8$^+$ T cells. C) Z-
861 scored DotPlot of marker expression for each CD8$^+$ T cell subcluster. D) Significantly increased
862 proportion of subcluster 0 (CXCR3^{lo} naïve like) in T1D pLN as determined by linear modeling with
863 donor age and CyTOF batch as covariates. E) Significantly increased percentage of naïve CD8$^+$ T cells
864 expressing CXCR3 found in an independent cohort of pLN donors by flow cytometry. P value for (E) is
865 the result of an ordinary one-way ANOVA with Tukey's multiple test correction.

866

867 **Figure 2. IL-15 is predicted to drive signatures of memory maintenance and effector function in**
868 **T1D.** A) Experimental workflow for scRNAseq of pLN. B) UMAP projection of total pLN cells, which
869 were subsetted to T cells, reintegrated with rpca, and reclustered, resulting in 19 T cell clusters (C).
870 D) Heatmap of Z-scored gene expression data showing a selection of DEGs between T1D donors and
871 ND donors across naïve, Teff, and Texh CD8$^+$ T cells. E) Network plot using DEGs in naïve CD8 T cells
872 showing enrichment of reactome pathways in T1D. F) Network plot using DEGs in CD8 Teff cells
873 showing enrichment of reactome pathways in T1D. G) Network plot using DEGs in CD8 Texh cells

874 showing enrichment of reactome pathways in T1D. H) Compass plot of IREA results using the top
875 genes upregulated in T1D in naïve $CD8^+$ T cells ($p<0.05$, $log2FC>0.26$) as input. I) Compass plot of IREA
876 results using the top genes upregulated in T1D in $CD8^+$ Teff cells ($p<0.05$, $log2FC>0.26$) as input. J)
877 Compass plot of IREA results using the top genes upregulated in T1D in $CD8^+$ Texh cells ($p<0.05$,
878 $log2FC>0.26$) as input. H-J) Bar height is indicative of enrichment score, while color corresponds to
879 FDR-adjusted P value (two-sided Wilcoxon rank-sum test), red or blue arcs indicate significant
880 positive or negative enrichment, respectively. Genes highlighted on heatmap (D) met log2FC cutoffs
881 of 0.26 and adjusted p-value cutoffs of 0.05. Pathway analysis was performed with the reactomePA
882 package and visualized if adjusted $p<0.1$ with the clusterprofiler package.

883

884 **Figure 3. Integrative receptor and gene expression analysis highlights an enriched naïve $CD8^+$ T cell**
885 **TCR cluster in T1D pLN.** A) Gene expression and TCR Graph vs Graph results for CoNGA clusters with
886 score <1. Left half of semicircle indicates gene expression cluster, right half of semicircle indicates
887 TCR cluster assignment. Bar plots indicate the relative proportion of T1D (orange) and ND (blue) cells
888 for the given cluster (left) and for the entire dataset (right), followed by the same for nPOD ID, where
889 each color represents a different donor. Top 9 differentially expressed genes are shown per cluster,
890 as well as TCR genes, and TCR sequence features[31] (TCRseq features panel, with red indicating higher
891 and blue indicating lower scores relative to the rest of the dataset). A panel of manually curated
892 marker genes shown is shown on the far right with red dots colored by mean expression and sized by
893 percent of cells expressing the gene. DEGs are determined by Wilcoxon test and scaled by adjusted
894 p value, where full height requires $p<10^{-6}$. Fold changes <2 are shown in grey. Difference in cluster
895 proportion assessed with two-way Fisher's exact test.

896

897 **Figure 4 Cross-tissue clone and phenotype sharing in human pLN and pancreas.** A) Processing
898 workflow of pancreatic slices where pancreas was embedded in agarose and sliced using a vibratome
899 to yield 150μm slices[81, 82], after which cells were processed to single cell suspension, selected for
900 $CD45^+$ cells, and run on the 10X Chromium controller as described in methods. B) UMAP of integrated
901 gene expression data (n=2 donors, pLN and pancreatic slices). C) Histological staining (obtained from
902 nPOD Aperio e-slide manager) of insulin (pink), glucagon (blue), and CD3 (brown) across pancreas tail
903 of the two donors with paired pancreatic slice and pLN data shows increased insulitis in new-onset
904 donor 6551. Scale bars are included in the upper left corner of each image and correspond to 10x
905 magnification and 101um for donor 6551, and 20x magnification and 50um for donor 6536. D)
906 Dotplot showing Z-scored gene expression per cluster in (B), with dot size corresponding to percent
907 of cells in the cluster expressing the marker. E) Barplot illustrating distribution of expanded clones
908 across clusters, with the majority of expanded clones localizing to memory $CD8^+$ T cell clusters 0 (CD8
909 Teff) and 2 (CD8 cytotoxic T lymphocytes [CTL]). F) Assessment of repertoire overlap across tissues
910 with the Morisita-Horn metric shows limited sharing across tissues. G) Alluvial plot subsetted to only
911 shared clones showing clonal sharing between clusters 5 (eTreg) and 9 ($ICOS^{hi}$ TCM), and 0 (CD8 Teff)
912 and 2 (CD8 CTL) across both clusters and tissues.

913 **Figure 5. Tissue-dependent gene expression programs of memory $CD8^+$ T cell populations.**

914 A) Barplot of percent of each cluster per tissue illustrates differential subset abundance of innate and
915 adaptive immune cells. B) Violin plots illustrating differential expression of *LEF1* and *SELL* in CD8 T
916 cells between tissues. C) Volcano plot of differentially expressed genes in cluster 0 (CD8 Teff) between
917 pancreatic slices and pLN. D) Volcano plot of differentially expressed genes in cluster 2 (CD8 CTL)

918 between pancreatic slices and pLN. DEGs were defined as log2FC>0.26 and corrected p value<0.05.
919 E) GSEA analysis of cluster 0 using Hallmark genesets. F) GSEA analysis of cluster 2 using Hallmark
920 genesets. GSEA analysis was performed using escape, and DE genesets were identified with a
921 Wilcoxon test. The top 20 gene sets with adjusted p <0.05 were plotted with positive fold change
922 indicating upregulation in pancreatic slice (orange) and negative fold change indicating upregulation
923 in pLN (blue).

924 **Figure 6. Naïve CXCR3$^+$ CD8 T cells possess features of stemness and polyfunctionality.** Flow
925 cytometry of cryopreserved pLN cells was performed to assess expression of canonical TSCM markers
926 and cytokine expression. A) Naïve CXCR3$^+$ (nCXCR3+) cells resemble TSCM and naïve cells in their
927 expression of TCF1. n=10, p values are the result of a repeated measures one-way ANOVA with
928 Tukey's multiple comparison test. B) Enrichment of TCF1$^+$ cells in naïve CXCR3+ cells as compared to
929 memory cells. N=10, p values are the result of a repeated measures Friedman test with Dunn's
930 multiple comparison test.C) TSCM and nCXCR3+ cells express more TOX as compared to naïve cells.
931 N=10, p values are the result of a repeated measures one-way ANOVA with Tukey's multiple
932 comparison test. D) T1D donor nCXCR3+ cells express enhanced TCF1 as quantified by stain index
933 [(median TCF1 expression in nCXCR3+ cells– median TCF1 expression in memory CD8 T cells)/(SD of
934 TCF1 in memory CD8 T cells * 2)] in nCXCR3+ cells from pLN. n=5 per group, p value is the result of a
935 two-tailed mann-whitney test. Upregulation of E) CD127, downregulation of PD-1 (F), and
936 upregulation of CD5 (G) in TCF1$^+$ compared to TCF1$^-$ cells. N=10, p values are the result of a two-tailed
937 t-test. H) nCXCR3+ cells possess, after 4 hours of PMA/ionomycin stimulation in the presence of
938 gologistop, more IL-2 and TNFα expressing T cells as compared to naive T cells, and more closely
939 resemble TSCM for expression of these molecules. n=10, p values are the result of a repeated
940 measures two-way ANOVA with Tukey's multiple comparison test.

941

942 **Figure 7. TCF1 and TOX co-expressing populations colocalize to the peri-islet area in human T1D.** A)
943 Schematic of phenocycler imaging of embedded pLN and pancreas from nPOD 6551. B)
944 Representative images of pancreas and pLN, with callouts showing TCF1 and TOX expressing
945 populations. C) Line plot illustrating the density of TCF1 and TOX expressing T cell populations across
946 islet distance, with TCF1 and TOX co-expressing cells having greater density nearer to the islets than
947 single positive populations. D) Representative islet images from donor 6551 showing lineage markers
948 (CD4, CD8) as well as TCF1, TOX, CD57 and PD1 alongside nuclear stain DAPI. E) Dotplot showing
949 expression of key memory, negative regulatory and activation related markers across TCF1 and TOX
950 expressing populations.

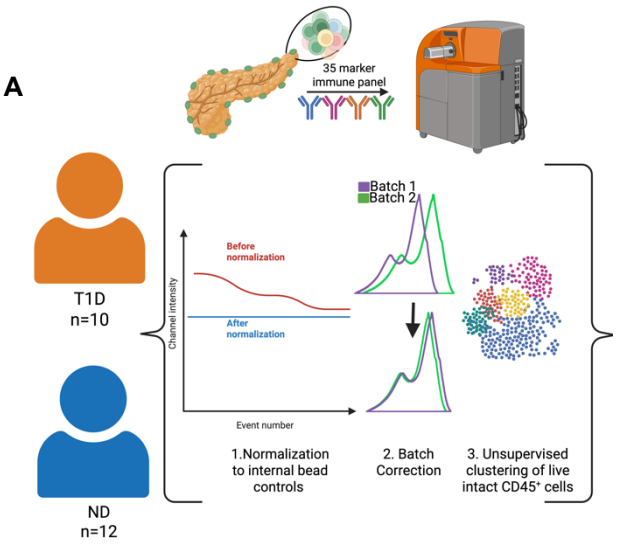
A
35 marker immune panel
T1D
n=10
ND
n=12
Batch 1
Batch 2
Before normalization
After normalization
Channel intensity
Event number
1.Normalization to internal bead controls
2. Batch Correction
3. Unsupervised clustering of live intact CD45⁺ cells

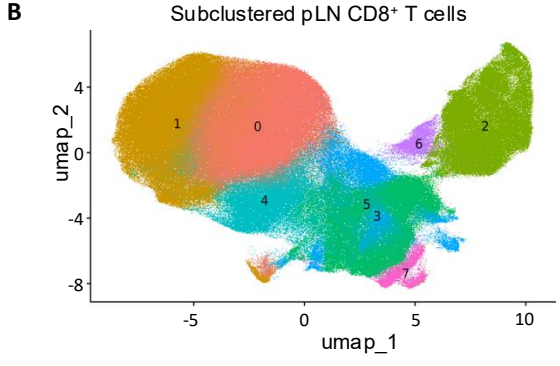
B
Subclustered pLN CD8⁺ T cells
umap_2
umap_1
0
1
2
3
4
5
6
7

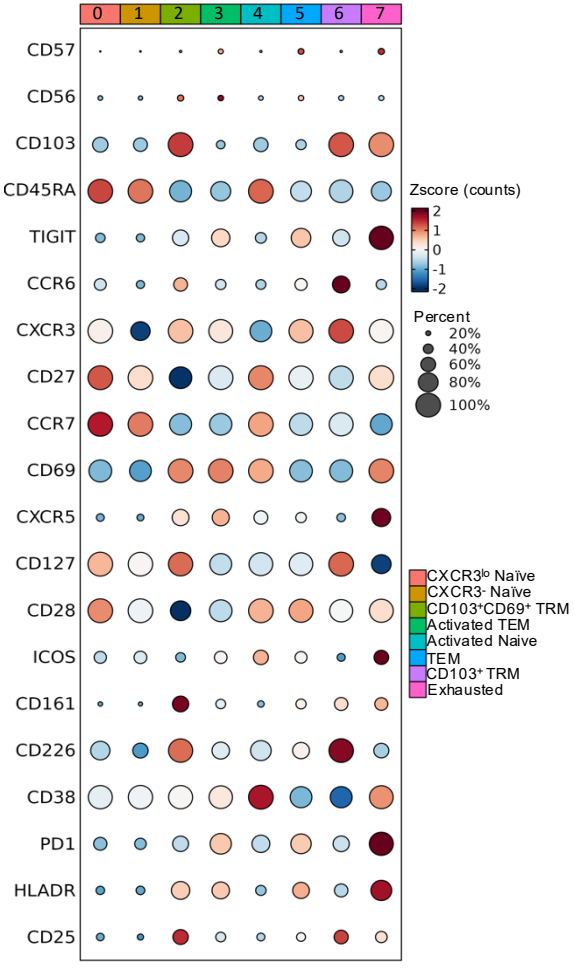
C
0
1
2
3
4
5
6
7
CD57
CD56
CD103
CD45RA
TIGIT
CCR6
CXCR3
CD27
CCR7
CD69
CXCR5
CD127
CD28
ICOS
CD161
CD226
CD38
PD1
HLADR
CD25
Zscore (counts)
2
1
0
-1
-2
Percent
20%
40%
60%
80%
100%
CXCR3lo Naïve
CXCR3- Naïve
CD103⁺CD69⁺ TRM
Activated TEM
Activated Naive
TEM
CD103⁺ TRM
Exhausted

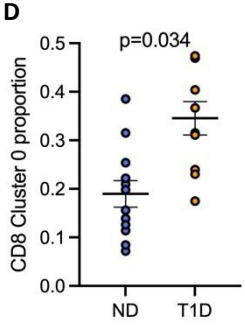
D
p=0.034
CD8 Cluster 0 proportion
ND
T1D

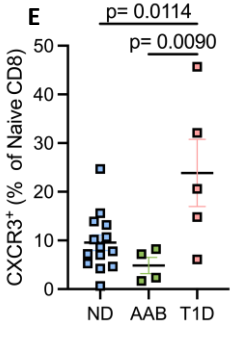
E
p= 0.0114
p= 0.0090
CXCR3⁺ (% of Naive CD8)
ND
AAB
T1D

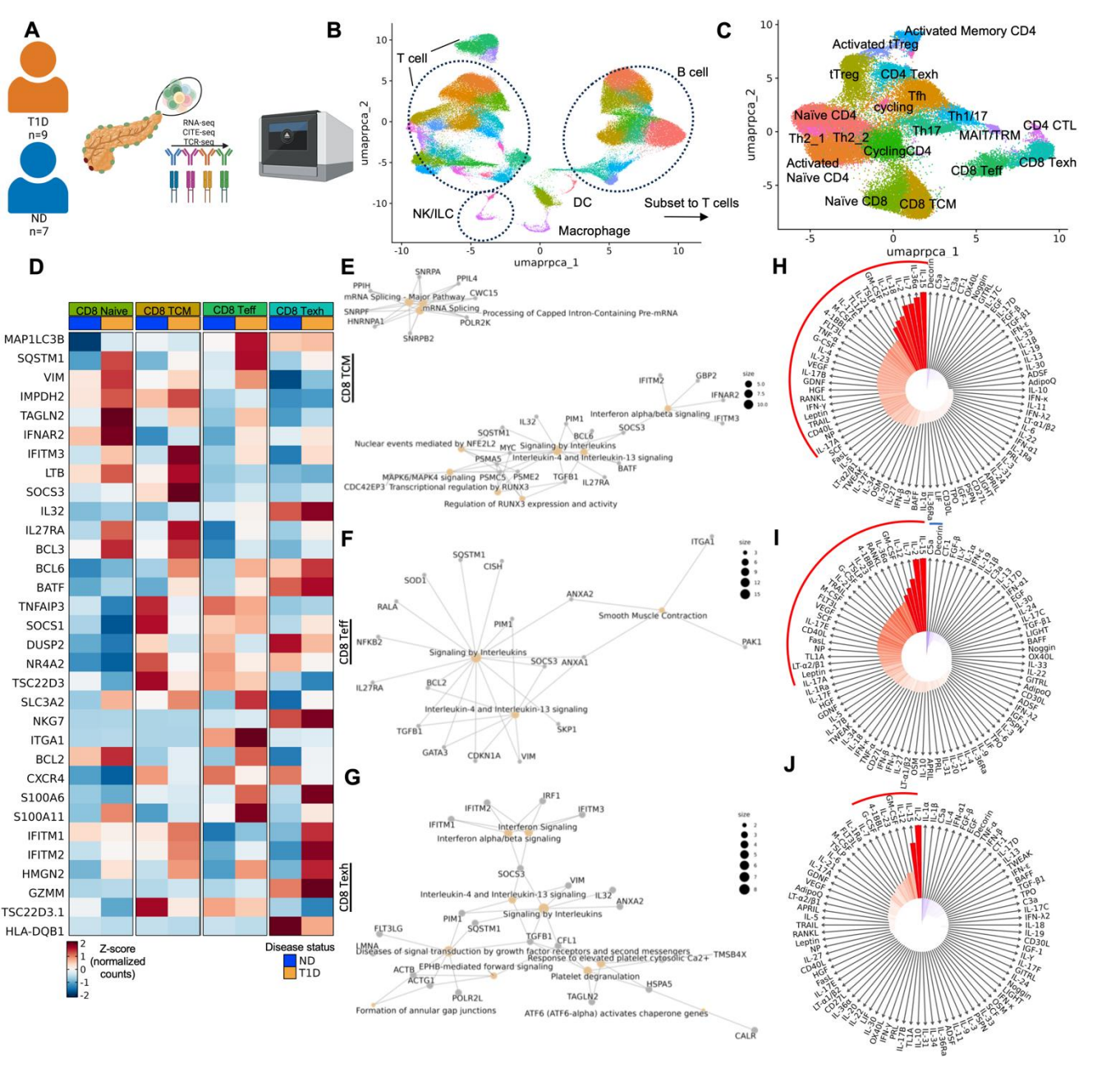
A
T1D
n=9
ND
n=7
RNA-seq
CITE-seq
TCR-seq
B
T cell
B cell
NK/ILC
DC
Macrophage
Subset to T cells
umaprpca_1
umaprpca_2
C
Activated Memory CD4
Activated tTreg
tTreg
CD4 Texh
Tfh
cycling
Naïve CD4
Th1/17
Th2_1
Th2_2
Th17
MAIT/TRM
CD4 CTL
CyclingCD4
Activated Naïve CD4
CD8 Teff
CD8 Texh
Naïve CD8
CD8 TCM
D
CD8 Naive
CD8 TCM
CD8 Teff
CD8 Texh
MAP1LC3B
SQSTM1
VIM
IMPDH2
TAGLN2
IFNAR2
IFITM3
LTB
SOCS3
IL32
IL27RA
BCL3
BCL6
BATF
TNFAIP3
SOCS1
DUSP2
NR4A2
TSC22D3
SLC3A2
NKG7
ITGA1
BCL2
CXCR4
S100A6
S100A11
IFITM1
IFITM2
HMGN2
GZMM
TSC22D3.1
HLA-DQB1
Z-score
(normalized
counts)
Disease status
ND
T1D
E
CD8 TCM
Signaling by Interleukins
Interleukin-4 and Interleukin-13 signaling
Interferon alpha/beta signaling
Regulation of RUNX3 expression and activity
F
CD8 Teff
Smooth Muscle Contraction
Signaling by Interleukins
Interleukin-4 and Interleukin-13 signaling
G
CD8 Texh
Interferon Signaling
Interferon alpha/beta signaling
Interleukin-4 and Interleukin-13 signaling
Signaling by Interleukins
Diseases of signal transduction by growth factor receptors and second messengers
Response to elevated platelet cytosolic Ca2+
Platelet degranulation
Formation of annular gap junctions
ATF6 (ATF6-alpha) activates chaperone genes
H
I
J

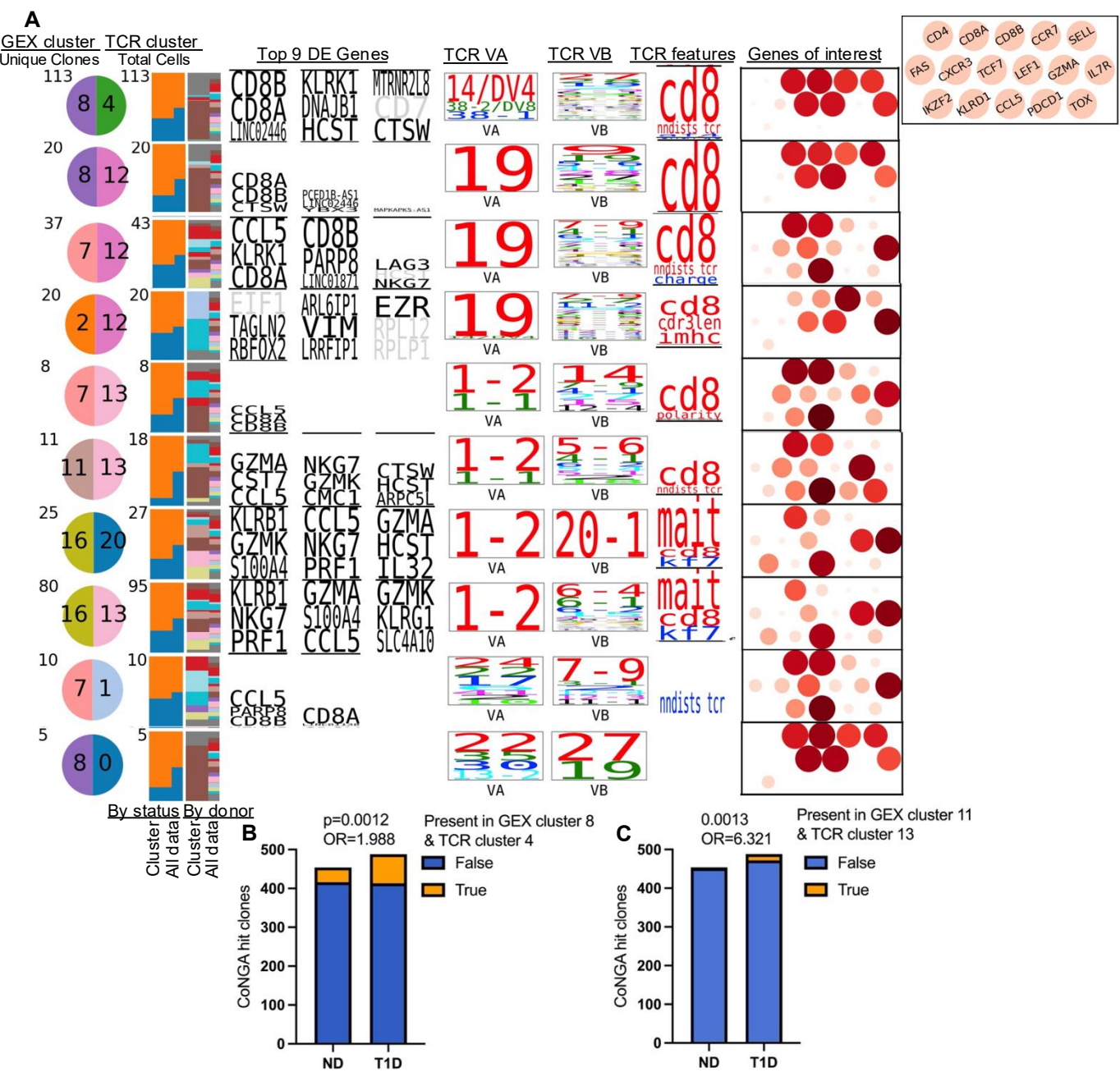
A
GEX cluster
TCR cluster
Unique Clones
Total Cells
Top 9 DE Genes
TCR VA
TCR VB
TCR features
Genes of interest
CD4
CD8A
CD8B
CCR7
SELL
FAS
CXCR3
TCF7
LEF1
GZMA
IL7R
IKZF2
KLRD1
CCL5
PDCD1
TOX
By status
By donor
Cluster
All data
B
p=0.0012
OR=1.988
Present in GEX cluster 8 & TCR cluster 4
False
True
CoNGA hit clones
ND
T1D
C
0.0013
OR=6.321
Present in GEX cluster 11 & TCR cluster 13
False
True
CoNGA hit clones
ND
T1D

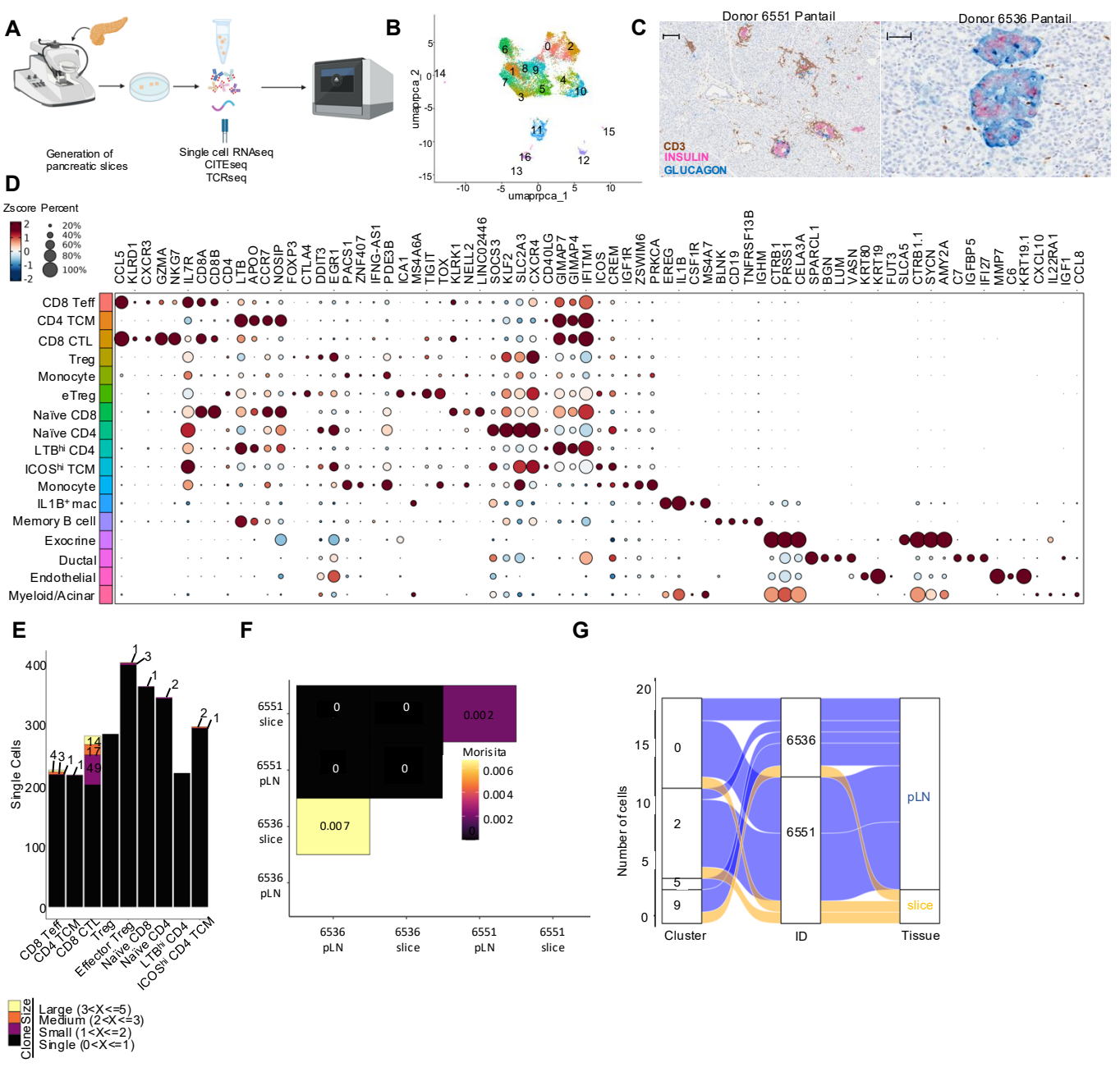
A
Generation of pancreatic slices
Single cell RNAseq
CITEseq
TCRseq
B
umaprpca_1
umaprpca_2
C
Donor 6551 Pantail
Donor 6536 Pantail
CD3
INSULIN
GLUCAGON
D
Zscore
Percent
CD8 Teff
CD4 TCM
CD8 CTL
Treg
Monocyte
eTreg
Naïve CD8
Naïve CD4
LTBhi CD4
ICOShi TCM
Monocyte
IL1B+ mac
Memory B cell
Exocrine
Ductal
Endothelial
Myeloid/Acinar
E
Single Cells
CD8 Teff
CD4 TCM
CD8 CTL
Treg
Effector Treg
Naive CD8
Naive CD4
LTBhi CD4
ICOShi CD4 TCM
CloneSize
Large (3<X<=5)
Medium (2<X<=3)
Small (1<X<=2)
Single (0<X<=1)
F
6551 slice
6551 pLN
6536 slice
6536 pLN
Morisita
G
Number of cells
Cluster
ID
Tissue
pLN
slice

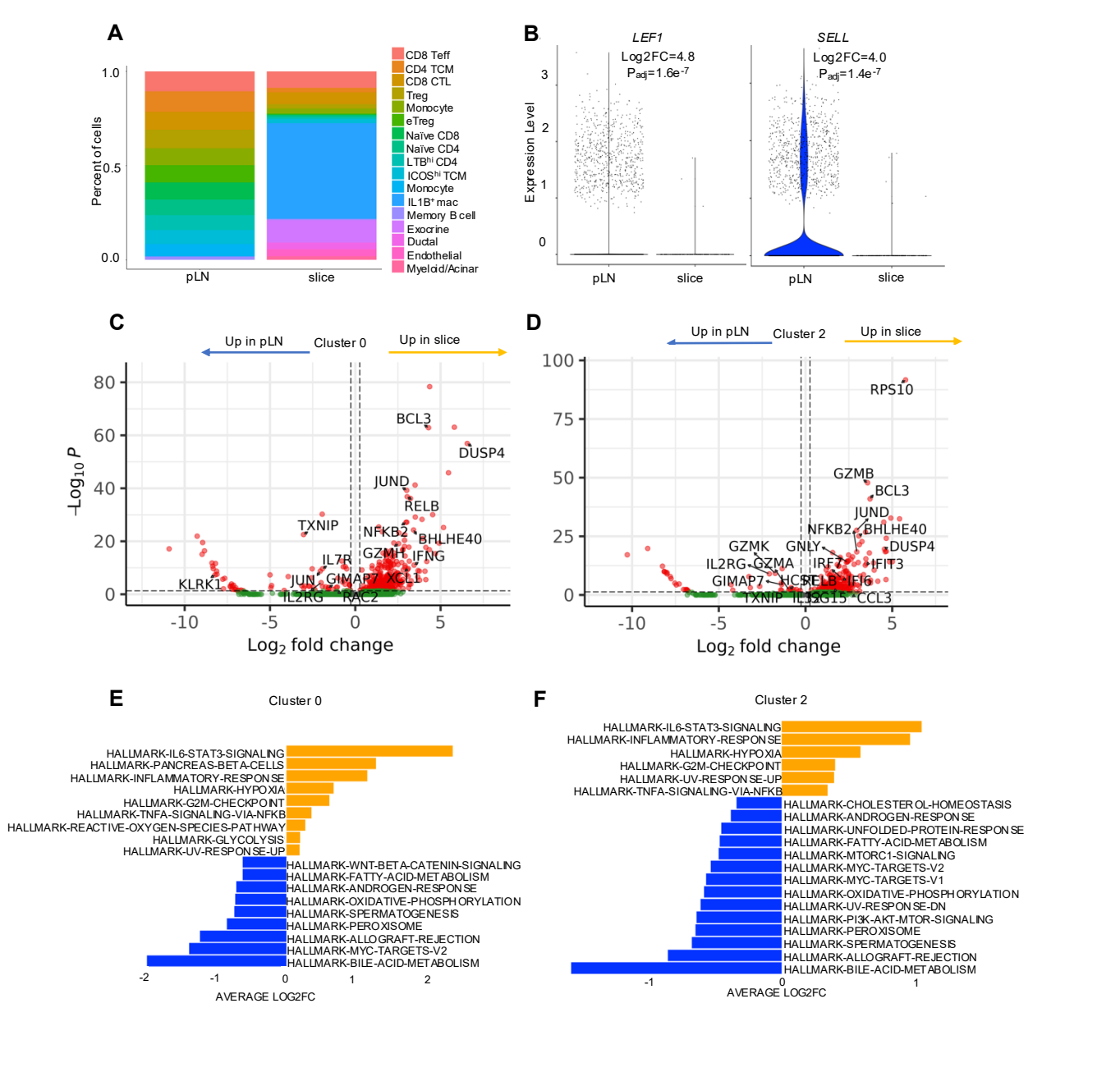
A
Percent of cells
1.0
0.5
0.0
pLN
slice
CD8 Teff
CD4 TCM
CD8 CTL
Treg
Monocyte
eTreg
Naïve CD8
Naïve CD4
LTB^hi CD4
ICOS^hi TCM
Monocyte
IL1B+ mac
Memory B cell
Exocrine
Ductal
Endothelial
Myeloid/Acinar
B
LEF1
Log2FC=4.8
Padj=1.6e-7
SELL
Log2FC=4.0
Padj=1.4e-7
Expression Level
pLN
slice
C
Up in pLN
Cluster 0
Up in slice
-Log10 P
Log2 fold change
BCL3
DUSP4
JUND
RELB
TXNIP
NFKB2
BHLHE40
GZMH
IFNG
IL7R
KLRK1
JUN
GIMAP7
XCL1
IL2RG
RAC2
D
Up in pLN
Cluster 2
Up in slice
Log2 fold change
RPS10
GZMB
BCL3
JUND
NFKB2
BHLHE40
DUSP4
GZMK
GNLY
IL2RG
GZMA
IRF7
IFIT3
GIMAP7
HCS
RELB
IFI6
TXNIP
IL32
IFG15
CCL3
E
Cluster 0
HALLMARK-IL6-STAT3-SIGNALING
HALLMARK-PANCREAS-BETA-CELLS
HALLMARK-INFLAMMATORY-RESPONSE
HALLMARK-HYPOXIA
HALLMARK-G2M-CHECKPOINT
HALLMARK-TNFA-SIGNALING-VIA-NFKB
HALLMARK-REACTIVE-OXYGEN-SPECIES-PATHWAY
HALLMARK-GLYCOLYSIS
HALLMARK-UV-RESPONSE-UP
HALLMARK-WNT-BETA-CATENIN-SIGNALING
HALLMARK-FATTY-ACID-METABOLISM
HALLMARK-ANDROGEN-RESPONSE
HALLMARK-OXIDATIVE-PHOSPHORYLATION
HALLMARK-SPERMATOGENESIS
HALLMARK-PEROXISOME
HALLMARK-ALLOGRAFT-REJECTION
HALLMARK-MYC-TARGETS-V2
HALLMARK-BILE-ACID-METABOLISM
AVERAGE LOG2FC
F
Cluster 2
HALLMARK-IL6-STAT3-SIGNALING
HALLMARK-INFLAMMATORY-RESPONSE
HALLMARK-HYPOXIA
HALLMARK-G2M-CHECKPOINT
HALLMARK-UV-RESPONSE-UP
HALLMARK-TNFA-SIGNALING-VIA-NFKB
HALLMARK-CHOLESTEROL-HOMEOSTASIS
HALLMARK-ANDROGEN-RESPONSE
HALLMARK-UNFOLDED-PROTEIN-RESPONSE
HALLMARK-FATTY-ACID-METABOLISM
HALLMARK-MTORC1-SIGNALING
HALLMARK-MYC-TARGETS-V2
HALLMARK-MYC-TARGETS-V1
HALLMARK-OXIDATIVE-PHOSPHORYLATION
HALLMARK-UV-RESPONSE-DN
HALLMARK-PI3K-AKT-MTOR-SIGNALING
HALLMARK-PEROXISOME
HALLMARK-SPERMATOGENESIS
HALLMARK-ALLOGRAFT-REJECTION
HALLMARK-BILE-ACID-METABOLISM
AVERAGE LOG2FC

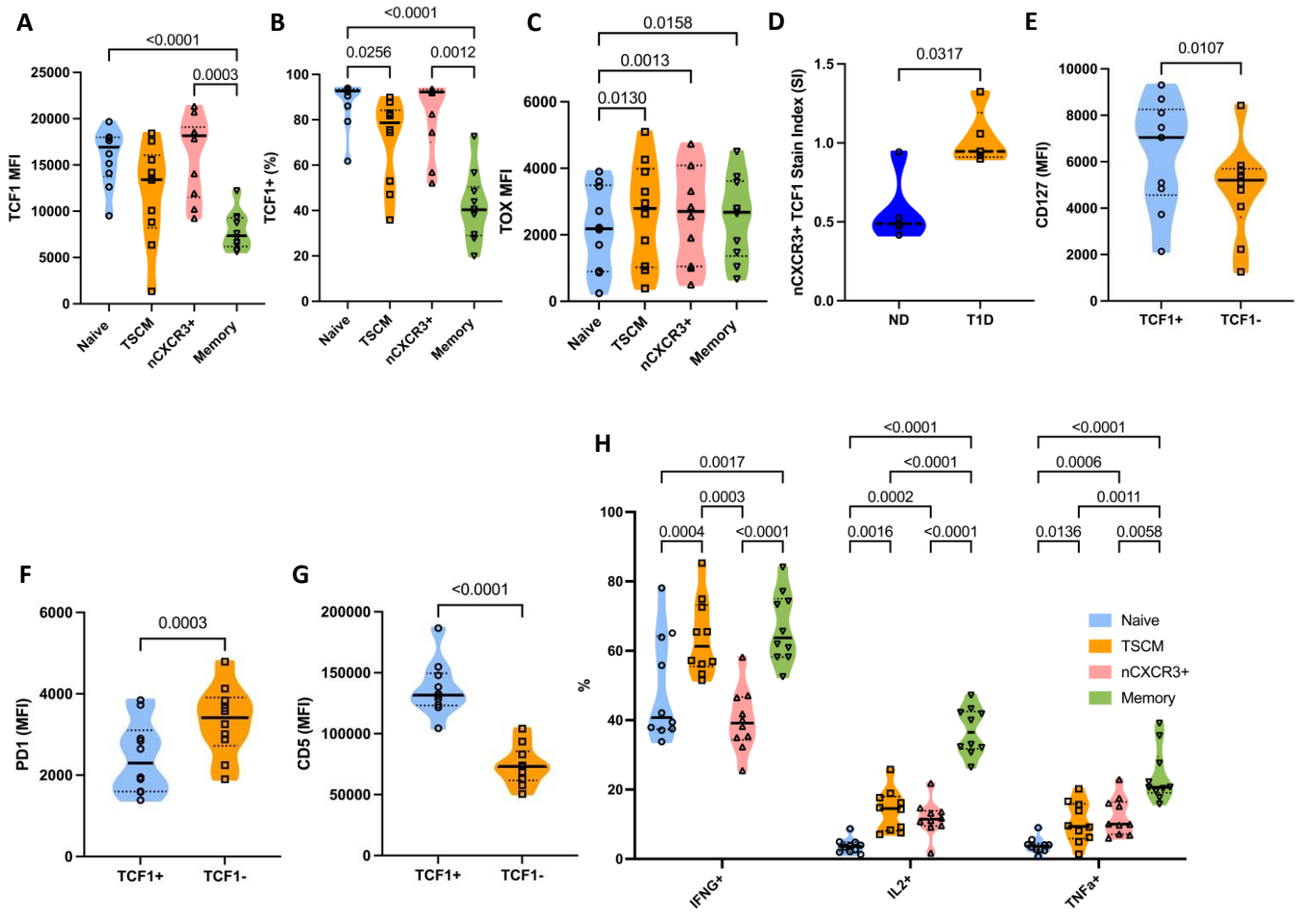
A
<0.0001
0.0003
TCF1 MFI
Naive
TSCM
nCXCR3+
Memory
B
<0.0001
0.0256
0.0012
TCF1+ (%)
C
0.0158
0.0013
0.0130
TOX MFI
D
0.0317
nCXCR3+ TCF1 Stain Index (SI)
ND
T1D
E
0.0107
CD127 (MFI)
TCF1+
TCF1-
F
0.0003
PD1 (MFI)
G
<0.0001
CD5 (MFI)
H
0.0017
0.0003
0.0004
<0.0001
<0.0001
<0.0001
0.0002
0.0016
<0.0001
<0.0001
0.0006
0.0011
0.0136
0.0058
%
IFNG+
IL2+
TNFa+

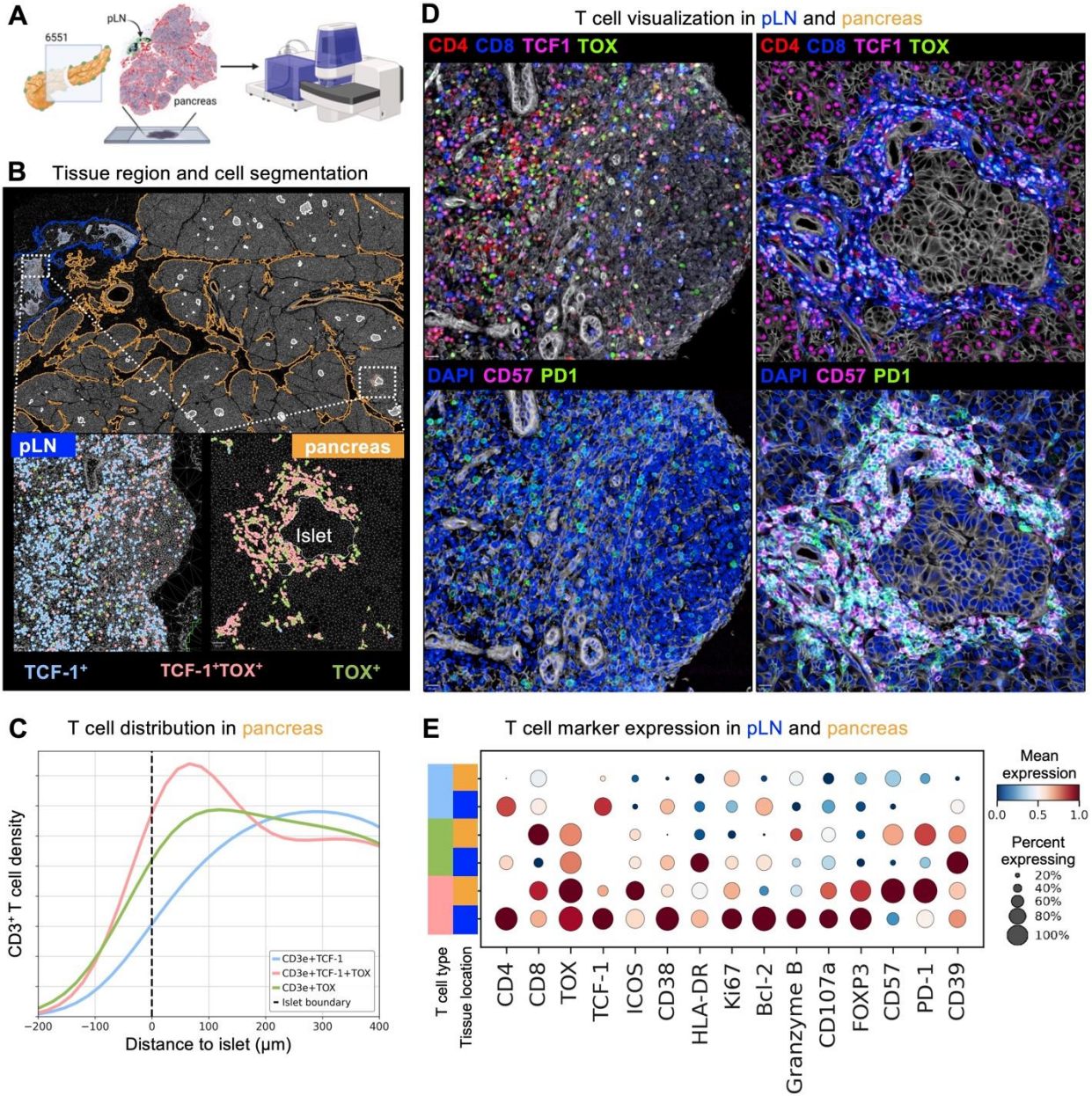
A
6551
pLN
pancreas
B
Tissue region and cell segmentation
pLN
pancreas
Islet
TCF-1+
TCF-1+TOX+
TOX+
C
T cell distribution in pancreas
CD3+ T cell density
Distance to islet (μm)
CD3e+TCF-1
CD3e+TCF-1+TOX
CD3e+TOX
Islet boundary
D
T cell visualization in pLN and pancreas
CD4 CD8 TCF1 TOX
DAPI CD57 PD1
E
T cell marker expression in pLN and pancreas
Mean expression
Percent expressing
T cell type
Tissue location
CD4
CD8
TOX
TCF-1
ICOS
CD38
HLA-DR
Ki67
Bcl-2
Granzyme B
CD107a
FOXP3
CD57
PD-1
CD39